Tectonics

RESEARCH ARTICLE
10.1029/2019TC005828

Key Points:
- Amphibolite-facies metamorphism and plutonism in the Greater Caucasus basement took place ~330–310 Ma
- The Main Caucasus Thrust formed as a greenschist-facies shear zone during Caucasus Basin inversion and/or rifting (~190–135 Ma)
- The Main Caucasus Thrust may have helped facilitate a portion of at least 5–8 km of basement exhumation during Arabia-Eurasia collision

Supporting Information:
- Supporting Information S1
- Table S1
- Table S2
- Table S3
- Table S4
- Table S5
- Data Set S1
- Data Set S2
- Data Set S3
- Data Set S4
- Data Set S5

Correspondence to:
D. A. Vasey,
davasey@ucdavis.edu

Citation:
Vasey, D. A., Cowgill, E., Roeske, S. M., Niemi, N. A., Godoladze, T., Skhirtladze, I., & Gogoladze, S. (2020). Evolution of the Greater Caucasus basement and formation of the Main Caucasus Thrust, Georgia. *Tectonics*, *38*. https://doi.org/10.1029/2019TC005828

Received 14 AUG 2019
Accepted 24 FEB 2020
Accepted article online 6 MAR 2020

Evolution of the Greater Caucasus Basement and Formation of the Main Caucasus Thrust, Georgia

Dylan A. Vasey[1], Eric Cowgill[1], Sarah M. Roeske[1], Nathan A. Niemi[2], Tea Godoladze[3], Irakli Skhirtladze[3], and Salome Gogoladze[3]

[1]Department of Earth and Planetary Sciences, University of California, Davis, CA, USA, [2]Department of Earth and Environmental Sciences, University of Michigan, Ann Arbor, MI, USA, [3]Institute of Earth Sciences, Ilia State University, Tbilisi, Georgia

Abstract Along the northern margin of the Arabia-Eurasia collision zone in the western Greater Caucasus, the Main Caucasus Thrust (MCT) juxtaposes Paleozoic crystalline basement to the north against Mesozoic metasedimentary and volcaniclastic rocks to the south. The MCT is commonly assumed to be the trace of an active plate-boundary scale structure that accommodates Arabia-Eurasia convergence, but field data supporting this interpretation are equivocal. Here we investigate the deformation history of the rocks juxtaposed across the MCT in Georgia using field observations, microstructural analysis, U-Pb and $^{40}Ar/^{39}Ar$ geochronology, and $^{40}Ar/^{39}Ar$ and (U-Th)/He thermochronology. Zircon U-Pb analyses show that Greater Caucasus crystalline rocks formed in the Early Paleozoic on the margin of Gondwana. Low-pressure/temperature amphibolite-facies metamorphism of these metasedimentary rocks and associated plutonism likely took place during Carboniferous accretion onto the Laurussian margin, as indicated by igneous and metamorphic zircon U-Pb ages of ~330–310 Ma. $^{40}Ar/^{39}Ar$ ages of ~190–135 Ma from muscovite in a greenschist-facies shear zone indicate that the MCT likely developed during Mesozoic inversion and/or rifting of the Caucasus Basin. A Mesozoic $^{40}Ar/^{39}Ar$ biotite age with release spectra indicating partial resetting and Cenozoic (<40 Ma) apatite and zircon (U-Th)/He ages imply at least ~5–8 km of Greater Caucasus basement exhumation since ~10 Ma in response to Arabia-Eurasia collision. Cenozoic reactivation of the MCT may have accommodated a fraction of this exhumation. However, Cenozoic zircon (U-Th)/He ages in both the hanging wall and footwall of the MCT require partitioning a substantial component of this deformation onto structures to the south.

Plain Language Summary Collisions between continents cause deformation of the Earth's crust and the uplift of large mountain ranges like the Himalayas. Large faults often form to accommodate this deformation and may help bring rocks once buried at great depths up to the surface of the Earth. The Greater Caucasus Mountains form the northernmost part of a zone of deformation due to the ongoing collision between the Arabian and Eurasian continents. The Main Caucasus Thrust (MCT) is a fault juxtaposing old igneous and metamorphic (crystalline) rocks against younger rocks that has often been assumed to be a major means of accommodating Arabia-Eurasia collision. This study examines the history of rocks along the MCT with a combination of field work, study of microscopic deformation in rocks, and dating of rock formation and cooling. The crystalline rocks were added to the margins of present-day Eurasia about 330–310 million years ago, and the MCT first formed about 190–135 million years ago. The MCT is likely at most one of many structures accommodating present-day Arabia-Eurasia collision.

1. Introduction

Collisional orogens are commonly characterized by basement-involved thrust faults or shear zones that develop as crustal-scale structures (e.g., Lacombe & Bellahsen, 2016; Lacombe & Mouthereau, 2002; Pfiffner, 2006). There are two mechanisms to explain the evolution of these structures in the conceptual framework of a singly-vergent, critically-tapered orogenic wedge, in which deformation is dominated by the translation of material along a shallowly-dipping basal décollement beneath an internally deforming fold-thrust belt (e.g., Chapple, 1978; Dahlen, 1984; Davis et al., 1983). The first involves the formation of a

basement-involved thrust by down-stepping of the basal décollement to deeper crustal levels and incorporating crystalline basement from the downgoing plate into the orogenic wedge (e.g., Lacombe & Bellahsen, 2016; McQuarrie, 2002), perhaps through normal-fault reactivation (e.g., Bellanger et al., 2014; Granado et al., 2017). The second mechanism produces a basement-involved thrust by the underthrusting of the wedge beneath the crystalline basement of the overriding continent, which serves as a backstop that limits back-thrusting and development of a retrowedge (e.g., Byrne et al., 1993; Rossetti et al., 2002). Investigating the evolution of basement-involved thrusts and the crystalline rocks they expose is thus essential for understanding the first-order structure of collisional mountain belts.

Between the Black and Caspian Seas, the Greater Caucasus Mountains are the locus of active shortening within the Arabia-Eurasia collision zone at their longitude (Jackson, 1992; Reilinger et al., 2006; Sokhadze et al., 2018). The range formed due to Miocene-Pliocene collision with the Lesser Caucasus to the south (Figure 1; e.g., Philip et al., 1989; Avdeev & Niemi, 2011; Cowgill et al., 2016). The Main Caucasus Thrust (MCT) is a north-dipping shear zone exposed in the core of the Greater Caucasus that, in the Republic of Georgia west of ~45°E longitude, juxtaposes Paleozoic crystalline rocks to the north against Mesozoic metasedimentary and volcaniclastic rocks to the south (Figure 1; e.g., Zaridze, 1959; Shempelev, 1978; Dotduyev, 1986; Saintot et al., 2006; Mosar et al., 2010).

The nomenclature of the MCT has also been extended to refer to an inferred Cenozoic basal décollement that is assumed to be the principal structure at depth accommodating Arabia-Eurasia convergence in the Greater Caucasus (e.g., Philip et al., 1989; Reilinger et al., 2006; Shempelev, 1978; Shempelev et al., 2017). Profiles across the range reveal a shift in crustal velocities within the upper ~10–20 km of the crust from higher velocities in the north to lower velocities in the south that has been tentatively interpreted as representing a crustal-scale décollement at depth, but the depth resolution of these profiles is insufficient to delineate the fault geometry clearly (e.g., Pavlenkova, 2012; Rogozhin et al., 2015; Shempelev, 1978; Shempelev et al., 2017). The correspondence of this inferred active décollement with the exposed shear zone observed within the range is generally implied by the shared name, but a correlation between these two structures has not been established.

In this study, we present structural, microstructural, geochronologic, and thermochronologic data from the surface exposure of the MCT and its corresponding hanging wall and footwall rocks in the Republic of Georgia. These data come specifically from two segments of the MCT separated by ~200 km along strike and known locally as the Ushba and Gveleti shear zones (Figures 2 and 3). Both shear zones define the southern margin of the crystalline core in the western Greater Caucasus and have been correlated to the surface trace of the MCT (e.g., Leonov, 1967; Shempelev, 1978).

Our data indicate that these shear zones likely formed prior to Arabia-Eurasia collision and appear to have played a relatively minor role in accommodating Cenozoic exhumation. U-Pb geochronologic analyses suggest that the Greater Caucasus crystalline core is an Early Paleozoic peri-Gondwanan terrane accreted onto the margin of Laurussia (Laurentia, Baltica, and Avalonia) during Late Paleozoic continental collision, resulting in widespread low-pressure/temperature metamorphism and plutonism. $^{40}Ar/^{39}Ar$ geochronology and thermochronology, together with microstructural observations, indicate that the Ushba and Gveleti shear zones formed during greenschist-facies deformation prior to Arabia-Eurasia collision. (U-Th)/He thermochronologic analyses indicate at least ~5–8 km of Cenozoic exhumation of the Greater Caucasus crystalline core in response to Arabia-Eurasia collision. However, Cenozoic (U-Th)/He cooling ages are also preserved in the footwall of the MCT, suggesting that a significant component of Cenozoic exhumation was accommodated on structures south of, and structurally below, the MCT. Thus, the crystalline rocks exposed in the hanging wall of the MCT appear to reflect the development of a backstop to the orogen in the western Greater Caucasus, rather than the expression of an active surface trace of the basal décollement that underlies the range.

2. Tectonic Setting

The present configuration of the Greater Caucasus is generally understood to result from Cenozoic closure of a Mesozoic back-arc basin (the Caucasus Basin) between the Greater Caucasus Paleozoic basement to the north and the Lesser Caucasus volcanic arc to the south during Arabia-Eurasia continental collision (Figure 1; Adamia et al., 1977; Zonenshain & Le Pichon, 1986; Gamkrelidze, 1986). From north

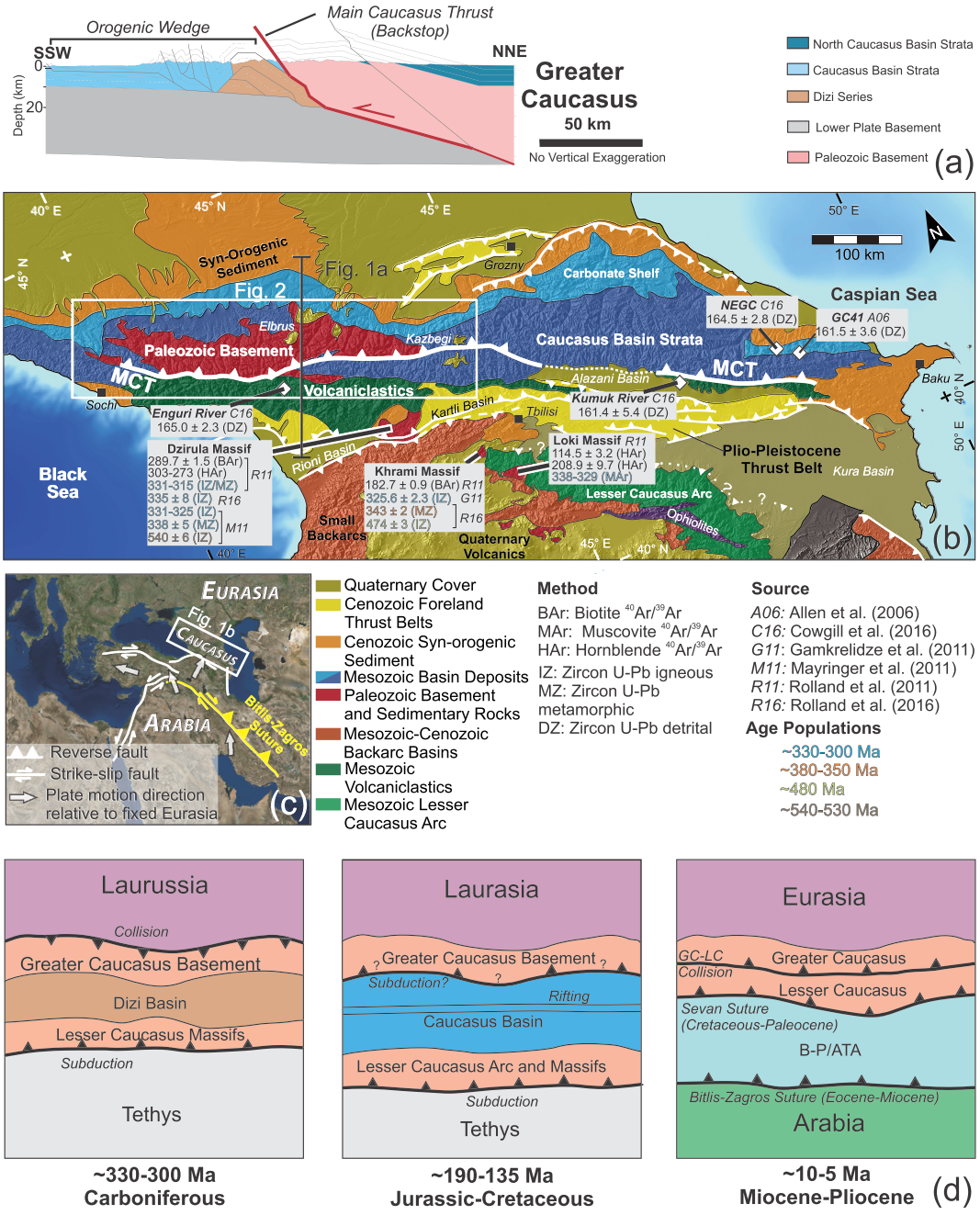

Figure 1. (a) Cross section showing major thrust faults in the Caucasus, including the Main Caucasus Thrust, modified from Trexler (2018). (b) Tectonic map of the Caucasus, modified from Cowgill et al. (2016). MCT = Main Caucasus Thrust. The numbers in gray boxes indicate ages in Ma (compiled from methods and sources in list below panel b) from Paleozoic crystalline rocks (Dzirula, Khrami, and Loki Massifs), Mesozoic sandstone (NEGC, GC41), and modern river sediment (Enguri and Kumuk Rivers). U-Pb detrital ages are youngest single-grain ages from these studies. (c) Map of Arabia-Eurasia collision zone showing major structures and approximate direction of plate motions relative to fixed Eurasia, modified from Cowgill et al. (2016). (d) Schematic maps illustrating key tectonic relationships discussed in the text, including Carboniferous accretion of the Greater Caucasus basement to Laurussia, Jurassic-Cretaceous evolution of the Caucasus Basin, and Miocene-Pliocene collision of the Greater (GC) and Lesser (LC) Caucasus. B-P = Bitlis-Pötürge block; ATA = Anatolian-Tauride-Armenian block.

to south, the major tectonic elements in the orogen relevant to this study are the Greater Caucasus Paleozoic crystalline core of metasedimentary, meta-igneous, and igneous rocks; the MCT; the Paleozoic to Triassic Dizi series of metasedimentary rocks; Mesozoic-Cenozoic clastic strata deposited in the Caucasus Basin; and the Paleozoic crystalline massifs of the Lesser Caucasus Mountains (Figures 1 and 2).

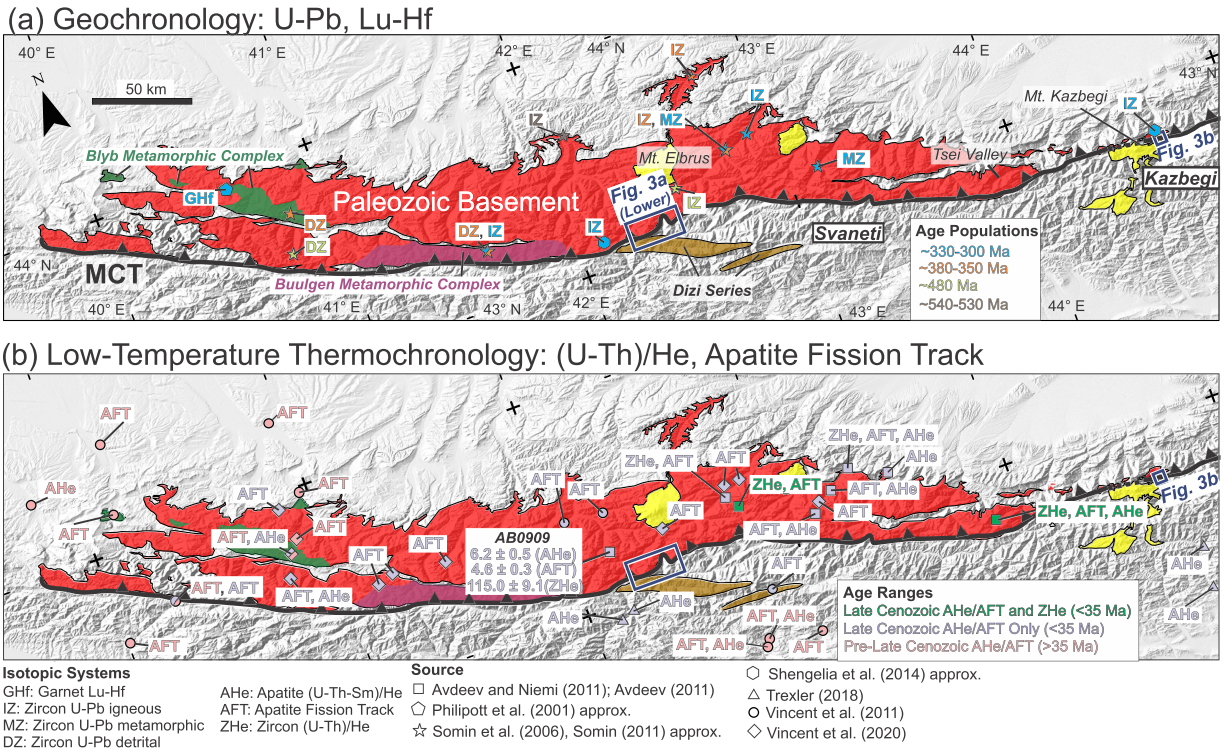

Figure 2. Map showing study areas (blue boxes) in the context of Paleozoic basement (red), the Paleozoic-Triassic Dizi series (brown), and modern volcanic centers (yellow), together with (a) ecolgite garnet Lu-Hf and zircon U-Pb geochronologic analyses and (b) low-temperature thermochronometric helium and apatite fission track analyses. Shading indicates the approximate location of the Blyb Metamorphic Complex (green) and Buulgen Metamorphic Complex (purple; Adamia et al., 2011; Somin, 2011). Color indicates age population. Letters indicate analysis type. Symbol indicates publication source. Approximately located samples indicated by "approx."

2.1. Arabia-Eurasia Collision

The Arabian plate is currently converging relative to Eurasia at a rate of ~20–30 mm/year (Reilinger et al., 2006). Between the Black and Caspian seas, the majority of the orogen-perpendicular component of this convergence is accommodated within the Greater Caucasus, as indicated by seismicity (Jackson, 1992), geodetic (Reilinger et al., 2006; Sokhadze et al., 2018), and geologic data (e.g., Adamia et al., 1977; Forte et al., 2010, 2014; Gamkrelidze, 1986; Mosar et al., 2010; Saintot, Brunet, et al., 2006). Timing of the onset of Arabia-Eurasia collision due to closure of the Neotethys Ocean along the Bitlis-Zagros suture is poorly constrained but typically interpreted to have occurred between the Eocene and Miocene (e.g., Agard et al., 2005; Hempton, 1985; McQuarrie & van Hinsbergen, 2013; Okay et al., 2010).

Final closure of the Caucasus Basin and collision between the Lesser and Greater Caucasus basements occurred in the Miocene-Pliocene, causing accelerated exhumation and growth of the present-day Greater Caucasus Mountains (Figure 1d; e.g., Mitchell & Westaway, 1999; Ershov et al., 2003; Mosar et al., 2010; Avdeev & Niemi, 2011; Cowgill et al., 2016; Vincent et al., 2020), although Oligocene growth of the range has also been argued for based on sedimentological data (Vincent et al., 2016, 2018). Present-day shortening appears to be dominantly concentrated in a south-directed foreland fold-thrust belt that deforms Mesozoic-Cenozoic strata along the southern margin of the Greater Caucasus in the Rioni, Kartli, Alazani, and Kura basins, with north-directed deformation on the north side of the range restricted to the central and eastern parts of the mountain belt (Figure 1b; e.g., Dotduyev, 1986; Banks et al., 1997; Mosar et al., 2010; Forte et al., 2010, 2013, 2014; Adamia et al., 2011; Trexler, 2018).

2.2. The Greater Caucasus Crystalline Core

West of 45°E, the core of the Greater Caucasus is composed primarily of Paleozoic igneous and metamorphic rocks exposed along and across strike for ~450 and ~50 km, respectively, that are typically inferred to

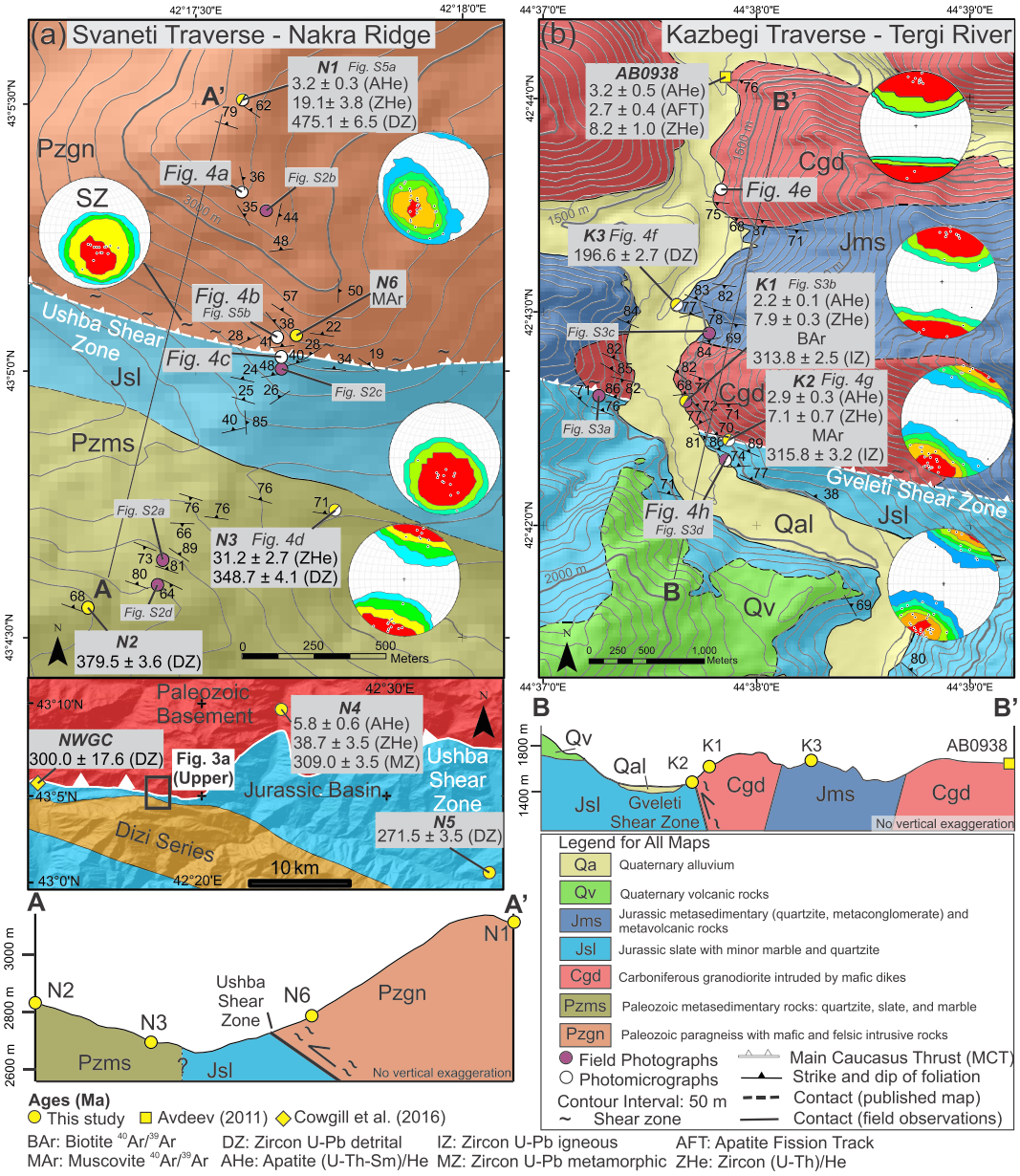

Figure 3. Geologic maps and cross sections based on 1:25,000-scale field observations and prior mapping. (a) Nakra ridge in the Svaneti region from our work, Gamkrelidze and Kakhazdze (1959), and Geguchadze et al. (1985). Area of detailed map is shown as black box in overview map. (b) Tergi River in the Kazbegi region from our work, Gubkina and Ermakov (1989), and Avrahamov et al. (1983). In a and b, the white circles indicate photomicrographs (Figures 4 and S5), the yellow symbols show radiometric analyses (Figures 5 and 6), and the purple circles indicate field photographs (Figures S2 and S3). U-Pb detrital ages are maximum depositional ages (this study) or youngest single-grain age (NWGC); U-Pb igneous/metamorphic ages are crystallization ages. Stereograms show foliation poles with Kamb contours in southern hemisphere projection (2σ contour interval, significance level of 3) for the major lithologic units on which they are placed and were generated using Stereonet v.10.1.0 (Allmendinger et al., 2011; Cardozo & Allmendinger, 2013).

represent the Greater Caucasus basement (Figures 1b and 2a; e.g., Adamia et al., 1977; Gamkrelidze, 1986; Somin, 2011). This crystalline core contains widespread granitoid plutonic rocks with ages of ~330-310 Ma that intrude Early-Middle Paleozoic metasedimentary and meta-igneous rocks (Figure 2a; Hanel et al., 1992; Somin et al., 2006; Somin, 2011; Shengelia et al., 2014; Kamzolkin et al., 2019), and the southern boundary of these crystalline rock exposures is commonly inferred to be a structural boundary, the MCT (Figure 1b; e.g., Zaridze, 1959; Dotduyev, 1986; Mosar et al., 2010; Somin, 2011). The tectonic affinity and deformation history of these crystalline rocks are key to understanding the Cenozoic assembly of the

Greater Caucasus, as well as the Phanerozoic evolution of the southern margin of Eurasia, but controversies remain regarding their age, evolution, and genesis (e.g., Mayringer et al., 2011; Somin, 2011; Ruban, 2013; Stampfli, 2013).

Two suites of rocks, the Blyb and Buulgen Metamorphic Complexes, have been alternately interpreted as Paleozoic sutures on the northern (Blyb; Mayringer et al., 2011; Somin, 2011) and southern (Buulgen; Adamia et al., 2011) margins of the crystalline core (Figure 2a). The Blyb Metamorphic complex contains garnet-whole rock Lu-Hf and Sm-Nd ages of ~330-300 Ma in eclogite, phengite $^{40}Ar/^{39}Ar$ ages of ~300 Ma in a kyanite-phengite-quartz vein, and Paleozoic serpentinite (Figure 2a; Perchuk & Philippot, 1997; Philippot et al., 2001; Somin, 2011). This high-pressure/temperature metamorphism and metamorphism of ultramafic rocks suggest that a Carboniferous suture may lie on the northern edge of the Greater Caucasus crystalline core (Figure 1d; Mayringer et al., 2011; Somin, 2011). In contrast, the Buulgen Metamorphic Complex contains a suite of amphibolite, metapelitic schist, and orthogneiss that has been interpreted as an ophiolitic accretionary complex (Figure 2a; Adamia et al., 2011; Stampfli, 2013), although this interpretation has been disputed (Somin, 2011).

A key component of unraveling the tectonic history of the crystalline core is determining whether these rocks originally formed on the margin of Gondwana and were accreted to the Laurussian East European Craton or formed on the margin of Laurussia. Fossil assemblages in Silurian, Devonian, and Carboniferous-aged sedimentary sequences on the northern flank of the Greater Caucasus but southeast of the Blyb complex are similar to those seen in European rocks interpreted to have formed on the margins of Gondwana prior to accretion to Laurussia (Kalvoda & Bábek, 2010; Ruban et al., 2007). A previous zircon U-Pb study of the crystalline core also noted the absence of Mesoproterozoic detrital zircons, which are also lacking in Gondwana-derived European terranes (Somin, 2011), but this absence is not significant given the low number of analyses (<35 grains/sample; Table S2 in the supporting information) and recent work on analysis statistics (Pullen et al., 2014).

2.3. The Main Caucasus Thrust (MCT)

The MCT is an orogen-length (~1,000 km), south directed thrust that runs along the contact between crystalline rocks to the north and Caucasus Basin strata to the south in the western Greater Caucasus and within Caucasus Basin cover strata in the eastern part of the range (Figure 1b; e.g., Zaridze, 1959; Dotduyev, 1986; Mosar et al., 2010; Somin, 2011). Although the MCT is often assumed to be an important Cenozoic structure (e.g., Dotduyev, 1986; Mosar et al., 2010; Philip et al., 1989; Reilinger et al., 2006), documenting the timing and magnitude of possible Paleozoic, Mesozoic, or Cenozoic deformation along it is crucial for understanding the role that this structure plays in the tectonic evolution of the Greater Caucasus orogen.

The precise location of the MCT is locally disputed or ambiguous. Where regional studies identify the trace of the MCT, generally without supporting field data, there is considerable inconsistency. In the Kazbegi region of Georgia (Figure 2), several early studies place the MCT along the Adaykom-Kazbek (or Adaykomskiy) fault, which broadly juxtaposes the crystalline Gveleti and Dariali massifs to the north against Caucasus Basin strata to the south (Leonov, 1967; Shempelev, 1978), whereas other studies place the MCT on the Tiba fault ~20 km to the south (e.g., Rogozhin et al., 2015; Vincent et al., 2018). Likewise, the location of the MCT is also disputed within the Caucasus Basin strata in eastern Greater Caucasus, with some authors placing it within the main range (e.g., Mosar et al., 2010; Vincent et al., 2018) and others on the Zangi fault farther to the south, at a major structural juxtaposition of differing Cretaceous facies (Cowgill et al., 2018; Forte et al., 2015; Khain et al., 2007; Kopp & Shcherba, 1985). In the western Greater Caucasus, the MCT footwall comprises either the Dizi series or Caucasus Basin strata, depending on location.

2.4. The Dizi Series

The Dizi series is a spatially restricted sequence of tightly folded, Devonian to Triassic, greenschist-facies metasedimentary rocks in the Svaneti region of Georgia (Figure 2a). This complex represents the only pre-Jurassic rocks reported in the Greater Caucasus in the immediate footwall of the MCT and has been previously dated with detailed biostratigraphy (Adamia et al., 2011, and references therein). The Dizi series consists primarily of slate and phyllite interbedded with minor quartzite, meta-conglomerate, marble, chert, and volcaniclastic rocks that has typically been interpreted as part of a marine basin that predated formation of

the Caucasus Basin (Adamia et al., 2011; Stampfli, 2013). The structural relationships between the Dizi series and both the crystalline rocks to the north and the Mesozoic strata to the south remain unclear (Somin, 2011).

2.5. The Caucasus Basin

The MCT footwall primarily comprises a Mesozoic-Cenozoic sequence of sedimentary and volcaniclastic rocks deposited in the Caucasus Basin, which is inferred to have initially opened in the Early Jurassic between the Greater Caucasus to the north and the Lesser Caucasus to the south (Figure 1; e.g., Zonenshain & Le Pichon, 1986; Saintot, Brunet, et al., 2006; Nikishin et al., 2011; Sosson et al., 2016). These rocks are locally metamorphosed, with slate, phyllite, marble, and quartzite reported south of the MCT in the western Greater Caucasus (e.g., Adamia et al., 1992). East of 45°E, where no crystalline core is exposed, Jurassic basin strata also make up the crest of the Greater Caucasus (e.g., Nalivkin, 1976). Mafic dikes of reported Early-Middle Jurassic age in Carboniferous crystalline rocks (e.g., Avrahamov et al., 1983; Gubkina & Ermakov, 1989) have been interpreted to reflect rifting during opening of the Caucasus Basin (Nikishin et al., 2011; Somin, 2000).

Possible Mesozoic deformation recorded in Caucasus Basin strata remains poorly understood. Angular unconformities at the Triassic-Jurassic boundary (Nikishin et al., 2011) and throughout Middle Jurassic strata of the Caucasus Basin (Egan et al., 2009; Leonov, 1969; Nikishin et al., 2011; Saintot, Brunet, et al., 2006) have been viewed as possible indicators of tectonic shortening. North of the crystalline core, subsidence modeling of well data and seismic sections from the Northern Caucasus basin likewise suggest periods of uplift and erosion in the Late Triassic and Middle Jurassic, as well as at the Jurassic-Cretaceous boundary (Ershov et al., 2003). These erosional events also correlate with reported regressions in the Caucasus Basin, which may have been influenced by local tectonic uplift (Ruban, 2007).

2.6. Crystalline Massifs of the Lesser Caucasus Mountains

To the south of the Greater Caucasus (Figure 1b) lie the Jurassic-Cretaceous Lesser Caucasus volcanic arc (e.g., Rolland et al., 2011), the deformed Cretaceous-Eocene Adjara-Trialet basin (e.g., Yilmaz et al., 2000), and a series of exposures of Paleozoic crystalline rocks with diameters of ~10-50 km that include the Dzirula, Khrami, and Loki massifs (e.g., Gemkrelidze et al., 2011). We broadly consider these tectonic units as part of the geographic Lesser Caucasus Mountains and avoid the use of the term "Transcaucasus," which has been inconsistently applied to these and other tectonic features in the Caucasus region (Banks et al., 1997; Forte et al., 2010). The crystalline massifs record magmatic events at ~540 Ma and ~480 Ma, as well as low-pressure/temperature metamorphism and magmatism at ~340-310 Ma (Figure 1b; Gamkrelidze et al., 2011; Mayringer et al., 2011; Rolland et al., 2011, Rolland et al., 2016). Given that similarly aged magmatic rocks have been reported in the Greater Caucasus (Figure 2a; Somin, 2011; Shengelia et al., 2014), these massifs have been speculated to share a Paleozoic tectonic history with the Greater Caucasus crystalline rocks north of the MCT (Mayringer et al., 2011; Okay & Topuz, 2016), but this correlation is not universally accepted (e.g., Rolland et al., 2016).

3. Methods

We employed a variety of field methods, microstructural analysis, and geochronologic and thermochronologic techniques to better understand the affinity and deformation history of the southernmost contact between Paleozoic crystalline rocks and Mesozoic metasedimentary and volcaniclastic strata in central and western Georgia. This boundary is the most commonly defined location of the MCT in the western Greater Caucasus (e.g., Dotduyev, 1986; Saintot, Brunet, et al., 2006; Somin, 2000). We focus our efforts on two ~10-km-long traverses separated along-strike by ~200 km in the western Svaneti and eastern Kazbegi regions of the Republic of Georgia (Figure 3). The MCT, as defined above, is represented on these traverses by the Ushba shear zone in Svaneti and the Gveleti shear zone in Kazbegi (Trexler, 2018). For each traverse, we present structural, microstructural, geochronologic, and thermochronologic analyses to understand the tectonic affinity of rocks exposed in the hanging wall and footwall of the MCT, as well as the extent and timing of quartz-plastic deformation and exhumation. We also provide additional analyses from the broader Svaneti region from rock types not represented on the main traverse that bear on a broader understanding of the tectonic evolution of the region (Figure 3a).

3.1. Structural Field Observations

We mapped major lithologic contacts at 1:25,000 scale, measured metamorphic foliation and lineation, and collected samples for microstructural, geochronologic, and thermochronologic analyses along the ridgeline between the Nenskra and Nakra Rivers in Svaneti and along the Tergi River in Kazbegi. Figure 3 shows geologic maps of the two traverses derived from integrating our field observations with existing 1:50,000 and 1:200,000 scale maps (Avrahamov et al., 1983; Gamkrelidze & Kakhazdze, 1959; Geguchadze et al., 1985; Gubkina & Ermakov, 1989), although we simplified stratigraphic subdivisions and ages due to inconsistencies between published maps.

3.2. Petrographic and Microstructural Analysis

We use petrographic and microstructural analyses of deformed rocks in thin section to assess overall deformation temperatures, as well as shear sense of ductile deformation, within the Ushba and Gveleti shear zones (Table S1 and Figures 4 and S5). We estimate maximum temperatures of deformation using a combination of mineral assemblages and quartzo-feldspathic deformation fabrics. In our metapelitic samples, we interpret metamorphic chlorite and biotite in the absence of higher-grade index minerals in metapelites to represent greenschist facies metamorphic conditions, typically in the range of ~300–500 °C. We interpret the presence of cordierite in these samples to be indicative of higher-grade, low-pressure/temperature amphibolite facies conditions of ~500–700 °C (Holdaway & Lee, 1977; Spear & Cheney, 1989). In quartzo-feldspathic rocks deformed at geological strain rates of ~10^{-14} s^{-1} to 10^{-12} s^{-1}, quartz dynamically recrystallizes at temperatures greater than ~300 °C, whereas feldspar tends to display dominantly brittle deformation up to temperatures of ~500 °C (Hirth & Tullis, 1992; Pryer, 1993; Stipp et al., 2002a, 2002b; Tullis & Yund, 1977). The mechanisms by which quartz dynamically recrystallizes change systematically with increasing temperature, with bulging (BLG) and subgrain rotation (SGR) recrystallization dominant between ~280 and 500 °C and grain boundary migration (GBM) dominant at greater than ~500 °C (Bailey & Hirsch, 1962; Hirth & Tullis, 1992; Stipp et al., 2002b; White, 1977). We thus use the presence of brittle feldspar deformation and quartz dynamic recrystallization mechanisms to provide additional constraints on deformation temperature.

3.3. Zircon U-Pb Analysis

To provide provenance data and radiometric age control on rock units along the MCT, we performed zircon U-Pb analyses on two igneous samples, five metasedimentary samples, and one mylonitic sample of unknown protolith (Tables 1 and S3 and Figure 5). Analyses were conducted at the Arizona LaserChron Center via laser ablation inductively coupled plasma mass spectrometry (LA-ICPMS) using an Element2 HR ICPMS, following analytical procedures outlined by Gehrels et al. (2006, 2008) and Gehrels and Pecha (2014). Additional details and weighted mean plots of crystallization, metamorphic, and maximum depositional ages produced using IsoPlot (Dickinson & Gehrels, 2009; Ludwig, 2008) are provided in the supporting information. We present resulting age distributions using both kernel density estimation and probability density plots generated by the DensityPlotter software (Figures 5, 7, and S8; Vermeesch, 2012). We also plot the combined results of Paleozoic-Jurassic Greater Caucasus U-Pb analyses as a cumulative age distribution (CAD) using the provenance R package of Vermeesch et al. (2016) to facilitate comparison with datasets from other regional source areas (Table S2 and Figures 7 and S8).

3.4. Mica $^{40}Ar/^{39}Ar$ Geochronology/Thermochronology

To assess the timing of quartz-plastic deformation along the MCT, we conducted $^{40}Ar/^{39}Ar$ analyses on one biotite and two muscovite separates from crystalline rocks in the Ushba (Svaneti traverse) and Gveleti (Kazbegi traverse) hanging walls and shear zones (Tables 1 and S4 and Figure 6a). Analyses were performed using a Nu Instruments Noblesse multicollector mass spectrometer at the Stanford University Noble Gas Lab following analytical procedures outlined in Coble et al. (2011) and Benson et al. (2017). Additional details are provided in the supporting information. Depending on textural evidence and qualitative estimates of peak temperature in the rocks, we interpret reported dates to reflect either mica crystallization during shear zone formation or cooling of preexisting mica below the closure temperatures of ~350 °C for biotite and ~425 °C for muscovite (Grove & Harrison, 1996; Harrison et al., 2009). The $^{38}Ar/^{39}Ar$ ratios for each step serve as a proxy for Cl/K, allowing identification of potential

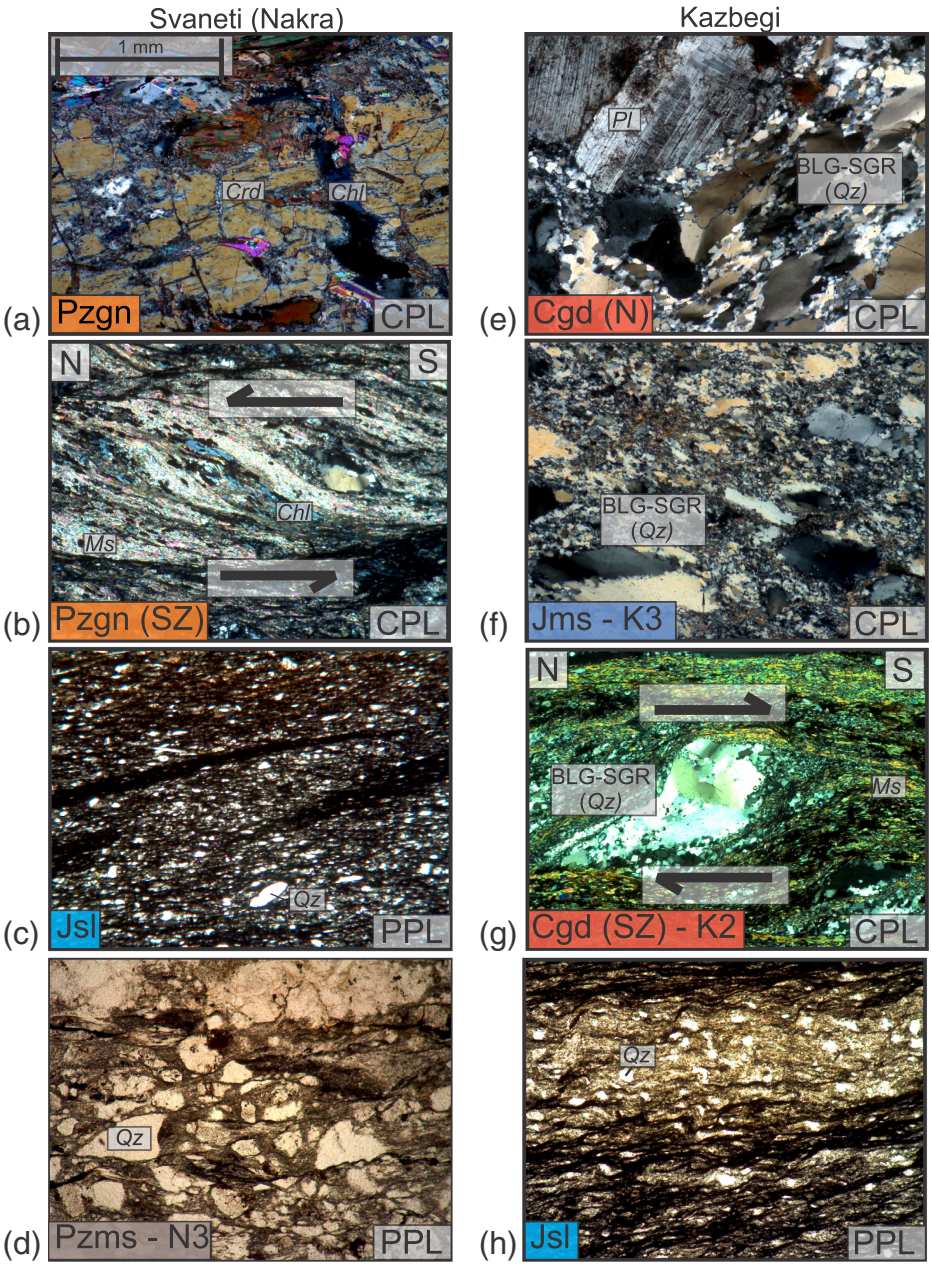

Figure 4. Representative photomicrographs from the (a–d) Svaneti and (e–h) Kazbegi traverses arranged from north (top) to south (bottom); SZ denotes the Main Caucasus Thrust (MCT) shear zone. Photomicrographs are shown at the same scale in either plane-polarized light (PPL) or cross-polarized light (CPL). Structural data for oriented photomicrographs are shown in Table S1. (a) Paleozoic paragneiss (Pzgn) with cordierite (Crd) porphyroblasts partially altered to chlorite (Chl). (b) MCT shear zone paragneiss that has been largely mylonitized to chlorite and muscovite (Ms) showing top-to-N shear. (c) Jsl slate with quartz (Qz) containing little evidence for dynamic recrystallization. (d) Paleozoic metasedimentary rocks (Pzms) with angular quartz clasts. (e) Carboniferous granodiorite (Cgd) with bulging (BLG) and subgrain rotation (SGR) dynamic recrystallization in quartz and brittle deformation in plagioclase (Pl). (f) Jurassic quartzite (Jms) with BLG-SGR quartz dynamic recrystallization. (g) MCT shear zone mylonitic fabric defined by elongate muscovite and quartz, with BLG-SGR quartz dynamic recrystallization and asymmetric quartz porphyroclasts showing top-to-S shear. (h) Jsl slate with no significant dynamic recrystallization in quartz.

multiple contributing phases (McDougall & Harrison, 1999; Villa et al., 2000, 2014). We present plots of step age and $^{38}Ar/^{39}Ar$ as a function of cumulative ^{39}Ar gas released using the IsoplotR software (Figure 6a; Vermeesch, 2018).

Table 1
Summary of Geochronology and Thermochronology Results

Sample	Full sample number	Lithology	Tectonic affinity	Latitude (°N)	Longitude (°E)	Elevation (m)	Zircon U-Pb age (Ma)[a]	$^{40}Ar/^{39}Ar$ total gas age (Ma)[b]	Zircon (U-Th)/He age (Ma)[c]	Apatite fission track age (Ma)[d]	Apatite (U-Th-Sm)/He age (Ma)[c]
Svaneti Traverse											
N1	C16014B	Paragneiss	Basement	43.09180	42.29313	3,126	475.1 ± 6.5 (D)	-	19.1 ± 3.8	-	3.2 ± 0.3[e]
N2	C16033B	Quartzite	Dizi Series	43.07594	42.28830	2,903	379.9 ± 3.2 (D)	-	-	-	-
N3	C16034B	Quartzite	Dizi Series	43.07898	42.29602	2,660	348.7 ± 4.1 (D)	-	31.2 ± 2.7	-	45.7 ± 20.9[f]
N4	CT15004B	Migmatite	Basement	43.16139	42.40510	1,818	309.0 ± 3.5 (M)	-	38.7 ± 3.5	-	5.8 ± 0.6
N5	100211-3A	Quartzite	Caucasus Basin	43.01184	42.59156	1,352	271.5 ± 3.5 (D)	-	-	-	-
N6	C16019	Paragneiss	Basement	43.08425	42.29470	2,889	-	133.8 ± 3.5 (Ms)	-	-	-
Kazbegi Traverse											
K1	V16046D	Granodiorite	Basement	42.70967	44.62780	1,434	313.8 ± 2.5 (C)	95.7 ± 2.5 (Bt)	7.9 ± 0.3	-	2.2 ± 0.1
K2	V16052A/B	Mylonite	Basement	42.70667	44.63115	1,522	315.8 ± 3.2 (C)	206.6 ± 5.4 (Ms)	7.1 ± 0.7	-	2.9 ± 0.3
K3	100711–3	Quartzite	Caucasus Basin	42.71721	44.62712	1,416	196.6 ± 2.7 (D)	-	-	-	-
Unpublished data from Avdeev (2011)											
	AB0909	Granite	Basement	43.24284	42.18634	2,400	-	-	115.0 ± 9.1	4.6 ± 0.3	6.2 ± 0.5
	AB0938	Orthogneiss	Basement	42.73501	44.63095	1,300	-	-	8.2 ± 1.0	2.7 ± 0.4	3.2 ± 0.5

[a]U-Pb crystallization (C), metamorphic (M), and maximum depositional (D) ages calculated using the weighted mean of the youngest population of ≥3 grains that overlap at the 2σ level (Dickinson & Gehrels, 2009). Errors reported at 2σ level. [b]Bt = biotite; Ms = muscovite. [c]Errors reported at 1 standard error. [d]Errors reported at 1σ level. [e]Sample mean age based on fewer than four individual apatite grain analyses. [f]Standard error on replicate grain ages exceeds 25%.

3.5. Zircon and Apatite He Thermochronology and Thermal Modeling

We present new zircon and apatite helium thermochronology data for five samples to assess spatial patterns of exhumation of the Greater Caucasus (Tables 1 and S5 and S6 and Figure 3). We also report previously unpublished helium and fission track thermochronology data for two samples from Avdeev (2011) (Tables 1 and S5–S7 and Figures 2 and 3). Additional details, including age corrections (Farley et al., 1996; Ketcham et al., 2011) and diffusion models (e.g., Flowers et al., 2009; Guenthner et al., 2013), are provided in the supporting information. Zircon (U-Th)/He (ZHe) ages are typically interpreted to represent cooling below ~180 °C (Reiners et al., 2004), whereas apatite (U-Th-Sm)/He (AHe) ages correspond to cooling below ~70 °C (Farley, 2000). ^{4}He was measured at the University of Michigan Thermochronology Lab using an Australian Scientific Instruments Helium Instrument (Alphachron) according to analytical procedures outlined in the appendix of Niemi and Clark (2018). Apatites were analyzed for U-Th-Sm content and zircons for U-Th content at the University of Arizona Radiogenic Helium Laboratory according to procedures described by Reiners and Nicolescu (2006). Three zircon and four apatite grains were analyzed per sample, except in cases where insufficient suitable grains were present or additional grains were run to compensate for low grain quality.

For samples with paired ZHe and AHe ages, we generated thermal history models using the QTQt software (v. 5.7.0C) of Gallagher (2012) to investigate the time-temperature histories of the samples (Figures 6b and S9 and S10). For one sample (K1), we present an additional thermal model that also incorporates thermal constraints from a biotite $^{40}Ar/^{39}Ar$ total gas age on that sample, using the diffusion parameters provided by Grove and Harrison (1996) to provide a first-order indication of the older/higher-temperature portion of the thermal history.

4. Results

4.1. Svaneti Traverse (West)

4.1.1. Field Observations

Along the Nakra ridge in Svaneti, we map the north dipping MCT contact (Ushba shear zone) as the juxtaposition of cordierite-mica paragneiss (Pzgn) in the hanging wall to the north against north dipping black

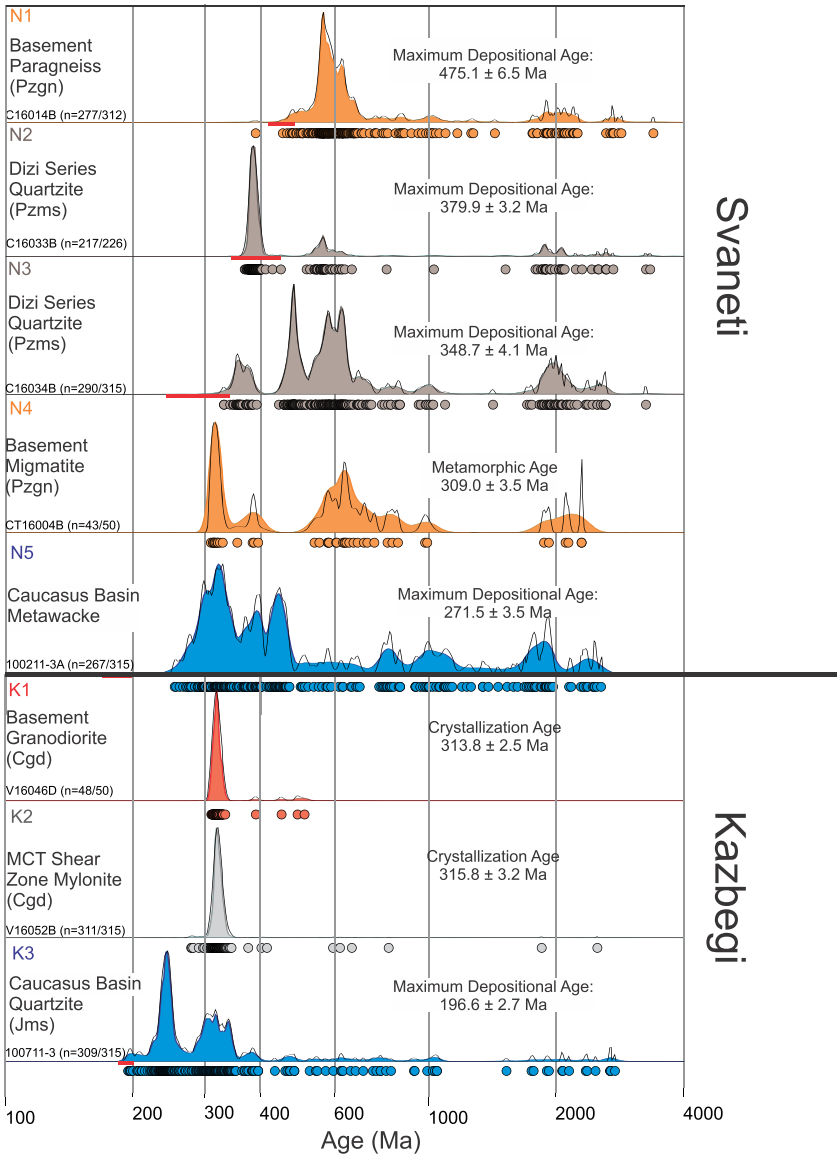

Figure 5. Kernel density estimates (KDEs—filled) and probability density plots (PDPs—outlines) on a logarithmic scale from 100 to 4000 Ma for zircon U-Pb analyses from the Svaneti and Kazbegi traverses. Samples are colored according to age and lithology (blue—Mesozoic metasedimentary; red—Paleozoic granitoid; brown—Paleozoic metasedimentary; orange—Paleozoic paragneiss; gray—mylonite). Circles indicate individual U-Pb analyses. The red bars show approximate depositional ages from Avrahamov et al. (1983) and Geguchadze et al. (1985). Original field sample numbers are followed by the number (n) of dates in parentheses (analyses accepted/total analyses performed).

slate (Jsl) in the footwall to the south (Figures 3a, 4a–4c, and S2a–S2c). The slate is juxtaposed to the south against a heterogeneous package of tightly folded, steeply north-northeast to south-southwest dipping quartzite, slate, and marble (Pzms), previously mapped as part of the Paleozoic-Triassic Dizi series (Figures 4d and S2d; Gamkrelidze & Kakhazdze, 1959; Geguchadze et al., 1985). It is unclear if the slate-Dizi series contact is depositional or a fault. In the hanging wall of the Ushba thrust, foliation attitudes in the paragneiss are variable but generally dip moderately to the northeast (Figures 3a and S4a). The Ushba shear zone is ~110 m thick in the hanging wall above the contact with the black slate (Jsl). Within this zone, foliation attitudes dip shallowly to the north, parallel to foliation in the underlying slate (Figures S4b and S4c). The paragneiss is mylonitized within the shear zone and hosts

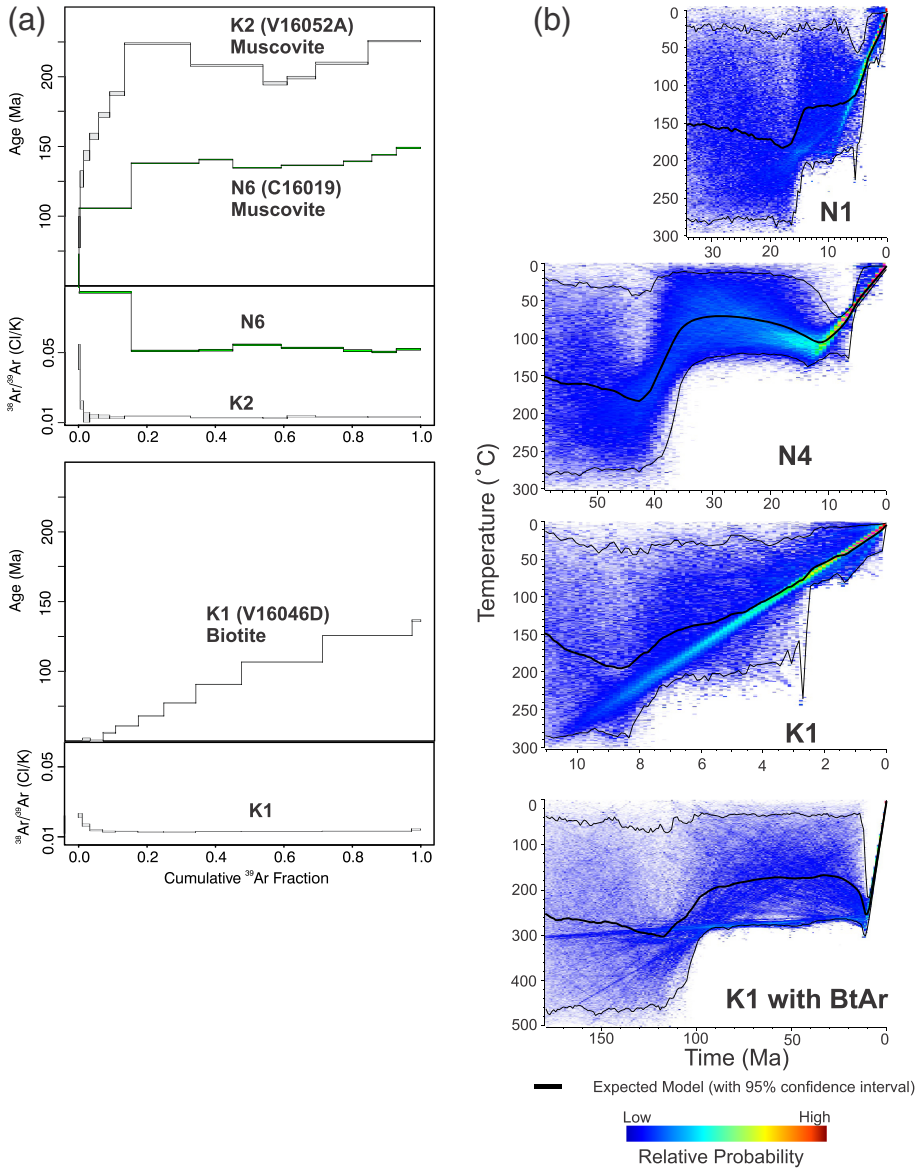

Figure 6. (a) ^{40}Ar/^{39}Ar step-release plots for muscovite and biotite analyses of samples N6, K1, and K2. The top panels show ^{40}Ar/^{39}Ar age, and the bottom panels show ^{38}Ar/^{39}Ar (taken as a proxy for Cl/K as explained in the text) vs. the cumulative fraction of ^{39}Ar released in a given step. Uncertainties are 1σ on plots of step ages. (b) QTQt thermal models of zircon (U-Th)/He and apatite (U-Th-Sm)/He data from samples N1, N4, and K1, as well as a second model of K1 incorporating biotite ^{40}Ar/^{39}Ar (BtAr) data with (U-Th)/He data. The blue boxes show thermal steps of lowest probability; the red boxes show steps of highest probability. The black line shows expected thermal model with 95% confidence envelope (see the supporting information for details).

an elevated concentration of quartz-calcite veins. Sparse mineral lineations trend north-northeast within the shear zone, in contrast to east-northeast in the overlying non-mylonitized paragneiss (Figures S4a and S4b).

4.1.2. Petrographic and Microstructural Analysis

Outside of the shear zone, the paragneiss consists of quartz, muscovite, and biotite, with limited cordierite porphyroblasts that are partially altered to chlorite and sericite (Figure 4a). Dynamically recrystallized amoeboid quartz grains ~100–200 μm in diameter indicate GBM recrystallization (Figure S5a). Rocks within the shear zone primarily contain quartz, sericite, chlorite, and brown mica and show evidence for bulging (BLG) quartz dynamic recrystallization with grain size <30 μm (Figures 4b and S5b). Asymmetric indicators of shear sense are inconsistent; a single sample within the shear zone contains an S/C fabric with

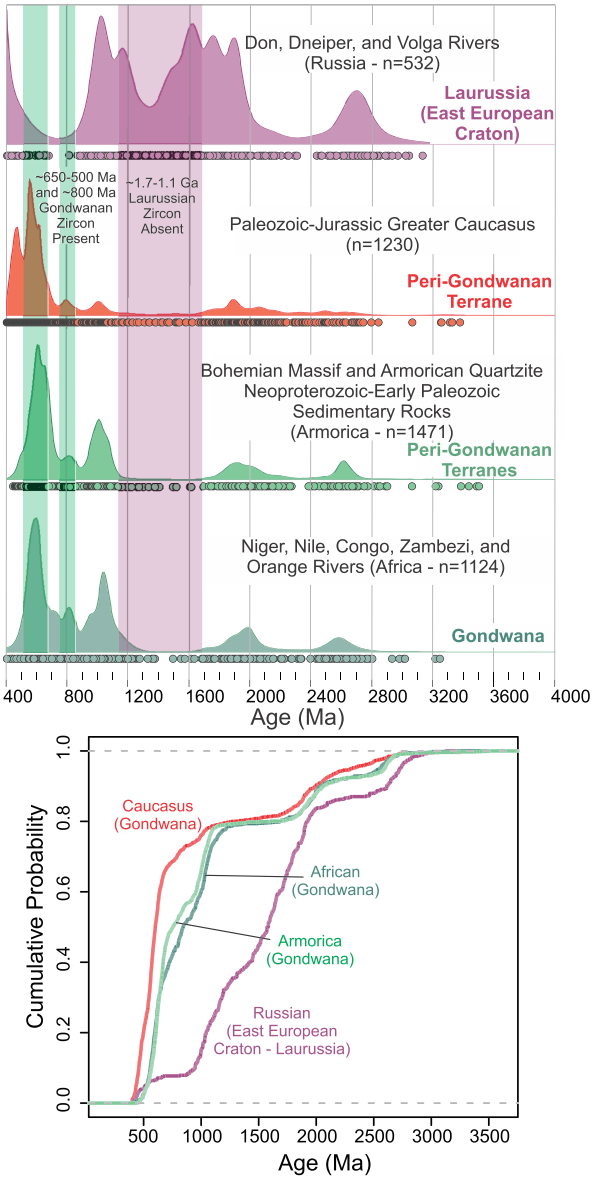

Figure 7. Zircon U-Pb ages plotted as kernel density estimation (KDE, top) and cumulative age distribution (CAD, bottom) curves showing similarity between the Greater Caucasus (red), Gondwana (dark green), and peri-Gondwanan terranes accreted to Laurussia (light green), all of which differ from Laurussia (purple). The green bars on the KDE indicate characteristic Gondwanan peaks that are well represented in the Greater Caucasus and poorly represented in Russian rivers. The purple bar on the KDE marks Laurussian peaks that are largely absent from the Greater Caucasus and Gondwanan sources. Curves show zircon U-Pb ages combined from Paleozoic-Jurassic samples in the Greater Caucasus (this study combined with Allen et al., 2006; Somin, 2011; Shengelia et al., 2014; Cowgill et al., 2016; Table S2), modern Russian rivers (Safonova et al., 2010; Wang et al., 2011) representing the East European Craton and Laurussia, modern African rivers (Iizuka et al., 2013) representing Gondwana, and Neoproterozoic-Early Paleozoic rocks of the Bohemian Massif and Armorican quartzite (Bahlburg et al., 2010; Drost et al., 2011; Shaw et al., 2014) representing peri-Gondwanan terranes. KDEs are plotted as in Figure 5 but on a linear scale from 400 to 4,000 Ma to highlight pre-Carboniferous histories. The CAD is plotted on a linear scale and only includes ages >400 Ma.

top-to-the-north (normal) shear sense (Figure 4b), whereas mica fish in samples outside of the high-strain shear zone suggest top-to-the-west (reverse) sense of rotation (Figure S5a). In the footwall, slate in unit Jsl consists of fine quartz, graphite, and minor muscovite. Within unit Pzms, quartzite contains quartz with minor plagioclase and muscovite, and marble consists of polysynthetic-twinned calcite and minor muscovite. Quartz grains in both footwall units Jsl and Pzms show no evidence of significant dynamic recrystallization, though the rocks do exhibit clear foliation in both outcrop and thin section (Figures 4c and 4d).

4.1.3. Zircon U-Pb Geochronology

We report zircon U-Pb analyses from five samples in the vicinity of the Ushba thrust (N1 and N4 in the hanging wall and N2, N3, and N5 in the footwall; Tables 1 and S3 and Figures 3a and 5). Detrital zircon analysis of hanging wall paragneiss (Pzgn sample N1) at Nakra ridge yields an Ordovician maximum depositional age of 475.1 ± 6.5 Ma, with significant age peaks at ~560 and ~620 Ma and a range of older ages up to ~3 Ga (Table 1 and Figures 5 and S7). Two quartzite samples from footwall unit Pzms along the Nakra ridge yield Devonian and Carboniferous maximum depositional ages of 379.9 ± 3.2 Ma (sample N2) and 348.7 ± 4.1 Ma (sample N3), respectively, consistent with prior assignment of this unit to the Dizi series. Additional significant age peaks are at ~480, ~560, and ~620 Ma, along with older ages up to ~3 Ga.

At the head of the Nakra valley, approximately ~10 km to the northeast of the Nakra ridge traverse, a migmatite within the hanging wall paragneiss (sample N4) contains a population of zircon grains with cores of lower U/Th ratio with ages that range from ~350 Ma to ~2.3 Ga and rims that contain high U/Th ratios (>100) dated to 309.0 ± 3.5 Ma (Table S3 and Figures 3a, 5, and S6). We were unable to date unit Jsl in the footwall on the Nakra ridge due to the lack of zircon in these rocks. However, quartzite (sample N5) collected from reported Early Jurassic sandstone (Gamkrelidze & Kakhazdze, 1959; Geguchadze et al., 1985) in the Enguri valley, ~30 km east of the Nakra ridge, yields a Permian maximum depositional age of 271.5 ± 3.5 Ma (Figures 3a, 5, and S7). Significant age peaks include ~300, ~320, ~380, and ~435 Ma, with older ages ranging up to ~2.5 Ga. All five samples show a pronounced lack of detrital zircon ages between ~1.1 and 1.7 Ga.

4.1.4. Mica $^{40}Ar/^{39}Ar$ Geochronology/Thermochronology

$^{40}Ar/^{39}Ar$ analysis of muscovite collected from paragneiss within the shear zone and ~25 m horizontally north of the Pzgn-Mzsl contact (sample N6) yields a complicated age spectrum, with a total gas age of 133.8 ± 3.5 Ma (Tables 1 and S4 and Figures 3a, 6, and S5c). Steps with ages older than 130 Ma comprise >80% released ^{39}Ar and yield ages broadly between ~135 and ~150 Ma with generally consistent $^{38}Ar/^{39}Ar$ (0.05 and 0.06); younger steps contain significantly higher $^{38}Ar/^{39}Ar$ (>0.08). The complexity of the age spectra prevents calculation of a clear plateau age by conventional metrics, which typically require that at least 50% of the released ^{39}Ar corresponds to ages indistinguishable at the 2σ level (Table S4 and Figure 6a; Dalrymple & Lanphere, 1974; McDougall & Harrison, 1999). Although the step ages >130 Ma in this sample are variable, they define a restricted age range of ~15 million years. The Cl/K values indicated by the $^{38}Ar/^{39}Ar$ measurements for these steps are similar and suggest minimal contamination by additional phases (Villa et al., 2014).

4.1.5. He Thermochronology and Thermal Modeling

Paired ZHe and AHe analyses from hanging wall paragneiss (N1) on the Nakra ridgeline yield ages of 19.1 ± 3.8 Ma and 3.2 ± 0.3 Ma, respectively (Tables 1 and S5 and S6 and Figure 3a). Thermal history modeling of the data from this sample (N1) using QTQt predicts cooling of ~20 °C/Myr starting from ~200-160 °C to surface temperatures over the last ~8-10 million years (Figure 6b). A second set of paired analyses from a migmatite (N4) in the MCT hanging wall in the Nakra valley, ~2 km horizontally north of the Ushba shear zone, yields ZHe and Aghe ages of 38.7 ± 3.5 Ma and 5.8 ± 0.6 Ma, respectively. Thermal history models of this sample (N4) indicate a period of negligible cooling or isothermal holding at ~110 °C from ~35 to 10 Ma, after which cooling accelerated to ~11 °C/Myr. Although the onset of accelerated cooling is similar for both models (~10 Ma), the younger ZHe age for N1 results in a post-10 Ma cooling rate that is about twice as fast as N4. Footwall quartzite (N3) ~1 km horizontally south of the Ushba shear zone on the Nakra ridge yields a ZHe age of 31.2 ± 2.7 Ma. AHe analyses from this sample yielded five individual grain ages ranging from ~9 to ~126 Ma, and the standard error on replicate grain ages exceeds 25%, indicating that the mean age is not statistically significant (Tables 1 and S6). Thermal models that include only the ZHe age of sample N3 are not well constrained enough to be geologically meaningful.

4.2. Kazbegi Traverse (East)

4.2.1. Field Observations

Along the Tergi River, the MCT (Gveleti shear zone) divides the Kazbegi map area into a southern domain of slate with minor quartzite and marble (Jsl) and a northern domain consisting of two exposures of granodiorite (Cgd) intruded by mafic dikes and separated by a metasedimentary unit (Jms) comprising quartzite, metaconglomerate, and metavolcanic rocks (Figures 3b and S3). The northern and southern crystalline bodies are the Dariali and Gveleti massifs, respectively. Foliation north of the Gveleti shear zone alternates between dipping steeply north and south, with south dips dominant (Figures S4e and S4f). The Gveleti shear zone is ~125 m thick north of the Cgd-Jsl contact and is characterized by mylonitization of the granodiorite, hydrothermal alteration, quartz veins, sparse down-dip lineations, and a dominantly steeply north-northeast dipping foliation that persists into the Jsl slate in the footwall (Figures 3b, 4g, S3a, and S4g and S4h.

4.2.2. Petrographic and Microstructural Analysis

Cgd granodiorite consists dominantly of quartz, plagioclase, highly-deformed biotite, and hornblende, with minor K-feldspar, chlorite, and sericite (Figure 4e). Metamorphosed mafic dikes within Cgd consist primarily of plagioclase, actinolite, epidote, and chlorite. Intervening Jms quartzite and metaconglomerate between the Dariali and Gveleti massifs consist dominantly of quartz, with minor muscovite in the quartzite (Figure 4f). Within Cgd and Jms, quartz grains have been dynamically recrystallized via bulging (BLG) and subgrain rotation (SGR), with recrystallized grain sizes of ~20–50 μm (Figures 4e–4g). Feldspar in the granodiorite is not dynamically recrystallized and shows evidence for brittle fracture (Figure 4e). Mylonite in the core of the shear zone consists primarily of quartz, white mica, and chlorite, with minor epidote, brown mica, and plagioclase (Figure 4g). Textural indications of original rock protolith have been largely erased. Some larger quartz and feldspar porphyroclasts contain asymmetric mantles indicating a top-to-the-south (reverse) shear sense (Figure 4g). Jsl slate to the south of the Gveleti thrust is foliated and contains quartz, graphite, minor chlorite, and minor muscovite; the quartz is angular and shows no evidence of dynamic recrystallization (Figure 4h).

4.2.3. Zircon U-Pb Geochronology

Hanging wall granodiorite (sample K1) yields a Carboniferous zircon U-Pb crystallization age of 313.8 ± 2.5 Ma, with a small number of inherited older zircon cores (Tables 1 and S3, and Figures 3b, 5, and S6 and S7). A large-n analysis of a shear zone mylonite (sample K2) of texturally ambiguous protolith (Figure 4g) yields a single-age peak of 315.8 ± 3.2 Ma, which is statistically equivalent to that of sample K1. Detrital zircon analysis of quartzite (sample K3) from unit Jms between the two granodiorite exposures produces an Early Jurassic maximum depositional age of 196.6 ± 2.7 Ma. Major age peaks occur at ~240, ~310, and ~330 Ma, with older ages up to ~2.7 Ga. This sample contains very few detrital zircons between the ages of ~1.1 and 1.7 Ga.

4.2.4. Mica $^{40}Ar/^{39}Ar$ Geochronology/Thermochronology

$^{40}Ar/^{39}Ar$ analysis of biotite from the granodiorite (K1) yields a staircase-pattern age spectrum with step ages ranging from ~25 to 140 Ma and a total gas age of 95.7 ± 2.5 Ma (Tables 1 and S4, and Figures 3b, 6a, and S5d). $^{38}Ar/^{39}Ar$ ratios are generally clustered between ~0.012 and ~0.014, with the youngest steps exhibiting

slightly higher ratios, up to ~0.022. Muscovite defining the foliation within the Gveleti shear zone (K2; Figure S5e) produces a complicated age spectrum with a total gas age of 206.6 ± 5.4 Ma. Initial steps systematically increase from ~90 to ~220 Ma and remaining steps range between ~190 and ~230 Ma. Steps younger than 140 Ma contain $^{38}Ar/^{39}Ar$ ratios >0.02, whereas older steps consistently range from ~0.012 to 0.014. Age spectra for both samples fail to define a conventional plateau age, but more than 80% of the released ^{39}Ar defines an age range of ~35 million years, and $^{38}Ar/^{39}Ar$ ratios suggest minimal contamination of these steps.

4.2.5. He Thermochronology and Thermal Modeling

In Kazbegi, paired ZHe and AHe analyses from granodiorite ~200 m north of the Gveleti thrust (K1) yield ages of 7.9 ± 0.3 Ma and 2.2 ± 0.1 Ma, respectively (Tables 1 and S5 and S6, and Figure 3b). Equivalent analyses from mylonitic shear zone sample K2 yield an overlapping ZHe age of 7.1 ± 0.7 Ma and slightly older AHe age of 2.9 ± 0.3 Ma. Modeling of K1 data predicts rapid cooling at ~28 °C/Myr since ~9 Ma from ~250 °C; the late Miocene ZHe ages preclude resolution of the thermal history prior to this time (Figure 6b). A second model of K1 incorporating the ~96 Ma biotite $^{40}Ar/^{39}Ar$ total gas age suggests that temperatures were unlikely to have exceeded ~300 °C since ~90 Ma, with rapid cooling at ~28 °C/Myr since ~10 Ma from ~280 °C. Modeling of K2 indicates cooling at ~31 °C/Myr since ~8 Ma from ~250 °C (Figure S9).

4.3. Combined Greater Caucasus U-Pb Geochronology

To establish the tectonic affinity of Paleozoic-Jurassic rocks exposed in the Greater Caucasus (Figures 7 and S8), we combine the 1,762 zircon U-Pb ages from this study with previously reported ages from crystalline basement rocks (Figure 2a; Somin, 2011; Shengelia et al., 2014), Mesozoic sandstone samples (GC41, NWGC, and NEGC; Figures 1b and 3a; Allen et al., 2006; Cowgill et al., 2016), and modern rivers draining the Greater Caucasus (Enguri, Kumuk; Figure 1b; Cowgill et al., 2016). Distinct age peaks in this compilation occur at ~240, ~310, ~380, ~480, ~560, and ~630 Ma, with subordinate older peaks at ~800 Ma, ~1 Ga, ~1.8 Ga, and ~2.5 Ga. Ages between ~1.1 and ~1.7 Ga are poorly represented, which is also indicated by the nearly flat slope of the cumulative area distribution (CAD) curve during this time interval (Figure 7).

5. Discussion

5.1. Age and Tectonic Affinity of the Greater Caucasus Basement

Previous faunal and detrital zircon U-Pb analyses have been interpreted to reflect that the Greater Caucasus crystalline core formed on the northern margin of Gondwana prior to accretion to Laurussia (Ruban et al., 2007; Somin, 2011). Our new zircon U-Pb analyses support a Gondwanan tectonic affinity for the Greater Caucasus. First, the combined pre-400 Ma zircon U-Pb ages for the Greater Caucasus do not match those of the modern Don, Volga, and Dneiper rivers currently draining the East European Craton (EEC). The zircon spectra derived from the EEC can reasonably be expected to represent the signature of Laurussia (Figure 7; Safonova et al., 2010; Wang et al., 2011). EEC-draining rivers are missing the significant age peak of 650–500 Ma grains pervasive in the Greater Caucasus, whereas grains with ages of 1.7-1.1 Ga found in these rivers are largely absent from the basement of the Greater Caucasus. Second, the grains with ages of 650-500 Ma found in samples from the Greater Caucasus are characteristic of rivers draining cratonic provinces of Gondwanan affinity in Africa (Iizuka et al., 2013). These African rivers also lack the grains with ages of 1.7-1.1 Ga typical of the East European Craton and contain age peaks around 2 and 2.5 Ga that are consistent with ages seen in the Greater Caucasus. Third, the zircon spectra of pre-400 Ma grains from the Greater Caucasus match the detrital zircon signatures of Late Proterozoic to Early Paleozoic sedimentary rocks in the Bohemian Massif of Central Europe and the Armorican Quartzite of Spain (Bahlburg et al., 2010; Drost et al., 2011; Shaw et al., 2014), both of which are widely viewed as Gondwana-derived units that accreted onto the Laurussian margin (Matte, 2001; Nance et al., 2010; Stampfli et al., 2013).

The Greater Caucasus also appears to share an Early Paleozoic tectonic affinity with the crystalline massifs of the Lesser Caucasus Mountains to the south. The ~540-Ma age of Cambrian intrusion in the Dzirula Massif is consistent with the major peak at ~650-500 Ma seen throughout the Greater Caucasus in this study (Figures 1b and 7; Mayringer et al., 2011). Additionally, an ~480-Ma peak observed in the Greater Caucasus zircon age spectra corresponds with an ~480-Ma magmatic signal reported in the Khrami Massif (Figures 1b and 7; Rolland et al., 2016). Crystallization ages of ~535–525 Ma and ~480–440 Ma comparable to those seen in the Dzirula and Khrami massifs have also been previously reported for igneous rocks farther to the north

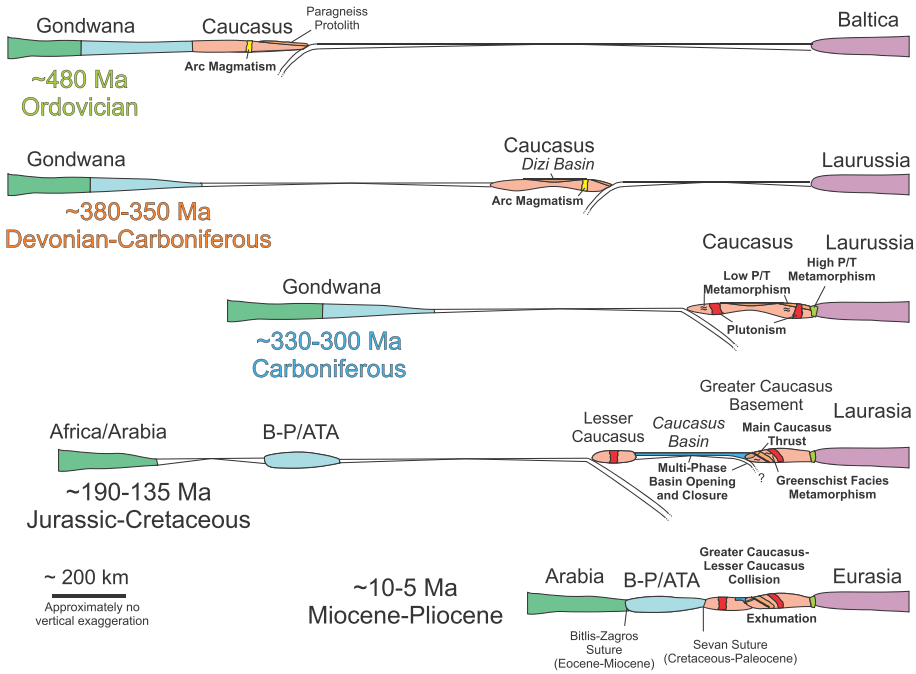

Figure 8. Schematic cross sections illustrating our preferred Phanerozoic tectonic evolution of the Greater Caucasus. The Caucasus rifted from Gondwana around the Ordovician (~480). The Dizi Basin opened within the Caucasus by the Devonian (~380 Ma). South directed subduction led to Carboniferous accretion of the Caucasus on the Laurussian margin (~330–300 Ma). Mesozoic changes in subduction dynamics within the Tethyan system caused alternating periods of rifting and basin inversion within the Caucasus Basin (~190–135 Ma), with the former separating the Lesser and Greater Caucasus basements and the latter likely resulting in formation of the Main Caucasus Thrust (MCT). The Miocene-Pliocene (~10–5 Ma) closure of the Caucasus Basin, collision between the Lesser and Greater Caucasus, and rapid exhumation of the Greater Caucasus basement occurred following the Eocene-Miocene collision of Arabia with the Anatolian-Tauride-Armenian (ATA) block and the Bitlis-Pötürge (B-P) block (Cowgill et al., 2016).

of our study area in the Greater Caucasus (Figure 2a; Somin, 2011). These ages of ~650-500 Ma and ~480 Ma correspond to similar ages in Gondwana-derived terranes in Central Europe and the Pontides that have been interpreted to represent orogeny and rifting on the Gondwanan margin (Linnemann et al., 2008; Nance et al., 2010; Okay et al., 2008). The Greater Caucasus and Lesser Caucasus contain zircon populations similar to those in Central Europe and the Pontides that likely reflect early Paleozoic orogenesis and rifting along the Gondwanan margin (Figure 8).

Maximum depositional ages of 379.9 ± 3.2 Ma (N2) and 348.7 ± 4.1 (N3) for samples purported, based on existing geologic mapping, to be from the Dizi series in Svaneti overlap with previously reported Silurian-Devonian and Carboniferous-Triassic biostratigraphic depositional ages for the same strata (Table 1 and Figure 5; Geguchadze et al., 1985). We interpret these maximum depositional ages as true Devonian (N2) and Early Carboniferous (N3) depositional ages, given their correspondence with biostratigraphic ages and their lack of zircon grains with ages of ~330-310 Ma (Middle-Late Carboniferous) that are prevalent in post-Carboniferous metasedimentary rocks reported in our study (i.e., N5 and K3; Figure 7). These Dizi series samples are similar to crystalline samples from the Svaneti traverse (N1 and N4), in that they also contain prominent age peaks at ~650–500 Ma and lack numerous grains between ~1.7 and 1.1 Ga. This zircon spectra fingerprint indicates that the Dizi series also shares a tectonic affinity with the northern Gondwana margin rather than the East European Craton.

5.2. Paleozoic Deformation in the Greater Caucasus

Rocks of the MCT region from this study record an amphibolite-facies metamorphic event preserved in the hanging wall of the Ushba shear zone along the Nakra ridge in Svaneti that likely dates broadly to ~330–310 Ma. In detail, this high-grade event is represented by cordierite-mica paragneiss (sample N1 from unit Pzgn) with GBM dynamic recrystallization and minor garnet-bearing granitoid intrusions (Figures 4a and S5a). These mineral assemblages and recrystallization textures indicate deformation at temperatures greater

than ~500 °C, and the presence of cordierite in particular suggests a low-pressure/temperature metamorphic event comparable to the ~330-Ma episode reported in the Dzirula and Khrami massifs (Mayringer et al., 2011; Rolland et al., 2016). The variable, moderately north to northeast dipping foliation in the amphibolite-grade paragneiss contrasts with the shallow, north dipping foliation seen in the Ushba shear zone and slate (Jsl) to the south (Figures 3a and S4a–S4c). We interpret this variably oriented foliation to represent the amphibolite-facies event. Migmatite in the Nakra valley (N4) contains ~310 Ma zircon rims with U/Th ratios >100, suggesting metamorphic zircon growth on older detrital cores of originally igneous zircon during low-pressure/temperature, amphibolite-facies metamorphism and partial melting of the paragneiss protolith at roughly this time (Table S3 and Figure S6; Vavra et al., 1996; Rubatto et al., 2009; Rubatto, 2017). Amphibolite-facies metamorphism of the Ushba hanging wall at ~310 Ma is coeval with a major phase of granitoid intrusion at ~330–310 Ma seen throughout the western Greater Caucasus and the Dzirula and Khrami Massifs of the Lesser Caucasus Mountains (Figures 1b and 2; Gamkrelidze et al., 2011; Mayringer et al., 2011; Somin, 2011; Shengelia et al., 2014; Rolland et al., 2016).

Along the Kazbegi traverse, this magmatic event at ~330-310 Ma is indicated by the ~315-Ma unimodal age peaks in the both the granodiorite in the MCT hanging wall (K1) and the Gveleti (MCT) shear zone (K2; Table 1 and Figure 5). We infer that the protolith of the shear zone mylonite (K2) was hanging wall granodiorite, based on the single-age peak resulting from analysis of more than 300 zircon grains. Although sample K2 lacks coarse biotite and plagioclase present in sample K1, K2 contains white mica, chlorite, epidote, brown mica, and minor microcrystalline plagioclase (~20 to 30μm in diameter) that we interpret as a retrograde metamorphic assemblage of the granodiorite.

The metamorphic and igneous zircon ages of ~330-310 Ma in the Greater Caucasus crystalline core and numerous detrital zircons in post-Carboniferous metasedimentary rocks (N5 and K3) correspond with the age of high-pressure/low-temperature metamorphism of eclogite at ~330-300 Ma in the Blyb Metamorphic Complex on the northern flank of the Greater Caucasus (Figures 2a and 5; Perchuk & Philippot, 1997; Philippot et al., 2001). Given that low-pressure/temperature metamorphism and plutonism at ~330-310 Ma have also been observed in the Lesser Caucasus massifs, this late Carboniferous deformation likely took place during accretion of both the Greater Caucasus basement and the crystalline massifs of the Lesser Caucasus Mountains onto the Laurussian margin to the north, with the Blyb complex representing a suture zone formed at that time (Figures 1d and 8). Accretion of the Caucasus onto the Laurussian margin prior to the Ordovician is precluded by the prominence of zircons with ages of 650-500 Ma and absence of zircons with ages of 1.7-1.1 Ga in paragneiss sample N1, which has a maximum depositional age of ~480 Ma. Similar patterns in the age spectra from Devonian-Carboniferous rocks of the Dizi series likewise suggest derivation of the Dizi series from Gondwana, rather than the Laurussian margin (Figure 7).

Detrital zircons ranging in age from ~380 to 350 Ma are found in all metasedimentary rocks in this study (Figure 5) from the Paleozoic Dizi series (N2 and N3) and from the Jurassic Caucasus Basin strata (N5 and K3). Additional detrital zircons and igneous rocks with ages of ~380 to 350 Ma have also been reported in the crystalline core of the Greater Caucasus (N4; Figure 2a; Somin, 2011). We interpret these zircons with ages of ~380-350 Ma to reflect likely south-directed Devonian-Carboniferous subduction and arc magmatism beneath the Caucasus prior to accretion on the Laurussian margin (Figure 8). In this scenario, the Dizi series may have been deposited in a minor back-arc basin forming between the Greater and Lesser Caucasus during this time (Figure 8). Northward subduction beneath the Caucasus could also be responsible for arc magmatism and back-arc basin formation (e.g., Adamia et al., 2011), but $^{40}Ar/^{39}Ar$ ages of 303–269 Ma from the Lesser Caucasus crystalline massifs have been interpreted to reflect the onset of north directed subduction following accretion (Figure 8; Rolland et al., 2011).

There may be an additional suture between the Greater Caucasus basement and the massifs of the Lesser Caucasus Mountains that formed prior to Carboniferous accretion onto the Laurussian margin, though we cannot resolve this with current data. The Buulgen Metamorphic Complex to the northwest of the Dizi series has been proposed as an ophiolitic complex (Figure 2; Adamia et al., 2011) that could define a Paleozoic suture between the Greater and Lesser Caucasus due to closure of the Dizi basin (Stampfli, 2013). However, Somin (2011) argued that the Buulgen complex may not be a true ophiolite due to the relative paucity of ultramafic rocks, the abundance of siliciclastic metasedimentary rocks, and overall dioritic composition of the magmatic rocks. The lack of high-grade metamorphism or Paleozoic magmatism in

Devonian-Carboniferous rocks of the Dizi series (N2–3) also suggests that convergence and/or crustal shortening across such a suture may have been relatively minor, although the size and tectonic history of the Dizi basin remain poorly understood.

5.3. Mesozoic-Early Cenozoic Formation of the Main Caucasus Thrust

In Svaneti, rocks in the Ushba shear zone exhibit BLG (~280–400 °C; Stipp et al., 2002b) dynamic recrystallization, along with S/C fabrics in which chlorite and muscovite dominantly define the S-bands (Figures 4b and S5b). Higher-temperature GBM dynamic recrystallization and amphibolite-facies mineral assemblages are confined to paragneiss north of the shear zone (N1; Figures 4a and S5a). We interpret these higher-grade fabrics and assemblages to reflect the Carboniferous accretion of the Greater Caucasus onto the Laurussian margin at ~330–310 Ma, given the ~310-Ma metamorphic overgrowths in migmatite sample N4 and the lack of younger metamorphic zircon rims in these samples. In Kazbegi, rocks in the hanging wall of the Gveleti shear zone contain transitional BLG-SGR (~400 °C) dynamic recrystallization (K1–K3; Figures 4e–4g), with asymmetric quartz porphyroclast mantling confined to the shear zone (K2; Figure 4g). No indications of amphibolite-facies deformation are seen along this traverse. As a result, we conclude that amphibolite-facies metamorphism and deformation predate formation of the MCT shear zone, which was formed during later greenschist-facies (~300–500 °C) metamorphism.

Along the Svaneti traverse, we interpret $^{40}Ar/^{39}Ar$ results from muscovite sample N6 within the Ushba shear zone to indicate that the MCT formed around ~150 to 135 Ma, based on the age range of steps with similar $^{38}Ar/^{39}Ar$ values (Figure 6a). The analyzed muscovite is generally part of the main foliation, suggesting that it crystallized during formation of the Ushba shear zone. However, Mesozoic-Cenozoic cooling of relict muscovite below the ~425 °C $^{40}Ar/^{39}Ar$ closure temperature cannot be ruled out (Harrison et al., 2009), given that muscovite also defines the older high-grade foliation in the paragneiss protolith to the north (Figures S5a and S5c).

Along the Kazbegi traverse, steps with similar $^{38}Ar/^{39}Ar$ values in sample K2 of fine-grained (45–300 μm) muscovite defining the foliation of the Gveleti shear zone yield ages of ~230–190 Ma (Figures 6a, 4g, and S5e). Zircon U-Pb analyses indicate that the protolith of sample K2 is likely igneous and formed at ~315 Ma (Figure 5), and there is no evidence for muscovite in samples of the protolith preserving igneous textures (K1; Figure 4e). As a result, we interpret these ages to reflect mica crystallization during shear zone formation rather than later resetting of the muscovite $^{40}Ar/^{39}Ar$ system. However, BLG-SGR (~400 °C) quartz dynamic recrystallization of sample K3 in unit Jms with a maximum depositional age of ~197 Ma clearly indicates that at least some component of quartz-plastic deformation took place in Kazbegi in the Early Jurassic or later (Figure 4f). We see two possible scenarios to reconcile these data.

The structurally simplest scenario is that the MCT formed in the Early Jurassic or perhaps later (i.e., after 197 Ma max deposition of sample K3), with the older $^{40}Ar/^{39}Ar$ steps in sample K2 reflecting relict muscovite, contamination by additional phases, or excess argon rather than MCT formation. The consistent $^{38}Ar/^{39}Ar$ values in sample K2 suggest minimal contamination by other phases, and we have observed no igneous muscovite in the likely protolith of sample K2 (Cgd; K1). The saddle-shaped age spectrum seen in sample K2 is often interpreted to reflect excess argon in biotite, feldspar, hornblende, and pyroxene (e.g., Kelley, 2002; McDougall & Harrison, 1999). If sample K2 contains excess argon, then the youngest age steps (~195 Ma) would provide only a maximum age of MCT formation. However, in muscovite, the youngest steps in saddle-shaped spectra have also been argued to reflect partial recrystallization of older muscovite during subsequent deformation events rather than excess argon (e.g., Alexandrov et al., 2002; Cheilletz et al., 1999).

Thus, an alternate scenario is that there were two quartz-plastic deformation events at Kazbegi, the first in the Triassic-Early Jurassic to form the MCT and older $^{40}Ar/^{39}Ar$ steps in sample K2, followed by a second event in the Early Jurassic or later to deform sample K3 and produce younger $^{40}Ar/^{39}Ar$ steps in sample K2. The portion of the Gveleti shear zone juxtaposing unit Cgd against Jsl could have formed during the older event, whereas the portion of the shear zone juxtaposing Jms against Jsl may have formed during the younger event, though we lack direct field observation of the Jms-Jsl contact (Figure 3b). The coarse quartzite and metaconglomerate in unit Jms are generally consistent with deposition in an active tectonic setting and may reflect this multi-part deformation.

Although we cannot definitively rule out Late Cenozoic quartz-plastic deformation in sample K3, we infer that this deformation was most likely Mesozoic or Early Cenozoic in age. Specifically, the dominantly Mesozoic to Early Cenozoic (~140 to ~50 Ma) stair-stepping biotite $^{40}Ar/^{39}Ar$ ages (with similar $^{38}Ar/^{39}Ar$) from the Kazbegi granodiorite in the hanging wall (K1) likely reflect prolonged residence of this sample in the biotite partial retention zone (~250–350 °C) during this time interval (Figure 6; Grove & Harrison, 1996; Reiners & Brandon, 2006). As a result, by the onset of Arabia-Eurasia collision, rocks now exposed at the surface had likely cooled to temperatures below those necessary for quartz-plastic deformation (~250 °C).

Alternating periods of back-arc rifting and basin inversion have been proposed throughout the Mesozoic development of the Greater Caucasus Basin, in large part on the basis of regional unconformities and hiatuses in sedimentation (e.g., Ershov et al., 2003; Nikishin et al., 2011). The MCT may have initially formed either as a reverse fault or as a normal fault that was later reactivated (Figure 8). Inconsistent shear sense indicators along the MCT between Svaneti (top-to-the-north; Figure 4b) and Kazbegi (top-to-the-south; Figure 4g) do not allow us to clearly discriminate between these two scenarios. The differences in muscovite $^{40}Ar/^{39}Ar$ ages in Svaneti (~135–150 Ma) and Kazbegi (~230–190 Ma) could indicate diachronous formation of the MCT, with the Ushba thrust in the west forming due to proposed basin inversion around the Jurassic-Cretaceous boundary (Nikishin et al., 2011) and the Gveleti thrust in the east forming earlier due to proposed Early and/or Middle Jurassic basin inversion (e.g., Ershov et al., 2003; Khain et al., 2007; Nikishin et al., 2011). Alternately, the Usbha and Gveleti shear zones could have formed synchronously in the Jurassic if the younger $^{40}Ar/^{39}Ar$ age from Svaneti reflects partial resetting resulting from later, post-Jurassic cooling.

The ages of ~230-190 Ma observed along the MCT in Kazbegi correspond with similar ages observed along sutures in East Asia and Iran (e.g., Kapp et al., 2003; Mirnejad et al., 2013; Pullen et al., 2008) typically associated with accretion of the Cimmerian continental ribbon on the margin of Laurasia (Metcalfe, 2013; Şengör, 1979). Although Triassic-Jurassic deformation and accretionary complexes have been identified in Turkey, debate persists regarding whether Cimmerian collision extended as far west as the Caucasus or whether such deformation reflects subduction accretion beyond the western edge of the Cimmerian fragment (Şengör, 2013; Topuz et al., 2013; Topuz et al., 2017), which has only been confidently traced as far west as northern Iran (e.g., Alavi, 1991; Natal'in & Şengör, 2005; Zanchetta et al., 2013). In this study, we do not observe any clear evidence in the Caucasus region for Triassic-Jurassic accretion of the Cimmerian ribbon, which if present would lie to the south of the crystalline massifs in the Lesser Caucasus, given the likely shared Carboniferous accretion of both the Greater Caucasus core and Lesser Caucasus massifs to Laurussia.

5.4. Late Cenozoic Exhumation of the MCT Hanging Wall and Shear Zone

Low-temperature AHe and ZHe thermochronometric analyses on both the Svaneti and Kazbegi traverses indicate Late Cenozoic exhumation of the MCT hanging wall from depths of at least ~5–8 km (Tables 1 and S5 and S6, and Figure 3). This exhumation may have been accommodated in part by brittle Cenozoic slip on the MCT, which is consistent with field observations of extensive hydrothermal alteration and abundant quartz veins along the Ushba and Gveleti shear zones. These data also suggest that some of this exhumation was likely due to Late Cenozoic slip on one or more additional major faults to the south of the MCT, as proposed by previous workers (e.g., Mosar et al., 2010). As explained below, thermochronometric data indicate limited if any Cenozoic greenschist-facies (i.e., quartz-plastic) shearing along the MCT, although it cannot be completely eliminated as a possibility.

In Svaneti, the muscovite $^{40}Ar/^{39}Ar$ ages of ~150-135 Ma from sample N6 in the greenschist-facies Ushba shear zone (Figures 4b and 6a) indicate that rocks along the shear zone likely remained below ~425 °C from the Cretaceous until the present, based on the muscovite $^{40}Ar/^{39}Ar$ closure temperature (Harrison et al., 2009). In the hanging wall of the Ushba shear zone, Eocene to Miocene ZHe ages (~40–20 Ma) coupled with Miocene-Pliocene AHe ages (~5–3 Ma) yield thermal models indicating a phase of slow to negligible cooling, starting as early as ~35 Ma in sample N4 or ~15 Ma in sample N1 and extending to ~10 Ma, followed by rapid cooling to surface temperatures from ~10 Ma to the present (Figure 6b). Younger thermochronometric ages in sample N1 compared to sample N4 require a slightly greater magnitude of cooling post-10 Ma for sample N1, from peak temperatures of ~160–200 °C instead of ~110 °C. This likely reflects the deeper structural

position of sample N1. These ZHe and AHe ages imply exhumation on the order of ~5–8 km since 10 Ma for the structurally deeper sample N1, assuming a typical geothermal gradient of 25–30 °C/km.

The $^{40}Ar/^{39}Ar$, ZHe, and AHe data from samples N1 and N6 limit the Cenozoic maximum temperature of the hanging wall and Ushba shear zone to be 160–425 °C prior to ~10 Ma. The higher end of this temperature range permits Cenozoic quartz-plastic deformation along the Ushba thrust and additional Cenozoic exhumation of up to ~9 km prior to ~10 Ma, assuming a geothermal gradient of ~25–30° km. When combined with the ~5–8 km of exhumation since 10 Ma, total Cenozoic exhumation of up to ~17 km is permissible, assuming a maximum of 425 °C at the beginning of the Cenozoic and a geothermal gradient of ~25–30 °C/km (Figure 6b). However, these thermochronometric ages do not allow us to further constrain the rate and timing of Cretaceous-Early Cenozoic exhumation.

A slight ZHe age offset is recorded across the Ushba shear zone, where the ~20-Ma ZHe age in the hanging wall paragneiss (N1) is younger than the ~31-Ma age in the footwall Dizi series (N3; Table 1 and Figure 3a). Thermal models of samples N1 and N4 suggest that age discrepancies within the hanging wall reflect different magnitudes of Late Cenozoic exhumation from different structural depths, rather than differences in the timing of exhumation. Differences in ZHe ages between the hanging wall and footwall of the Ushba shear zone likely reflect differences in the magnitude, rate, or timing of exhumation of these samples. In the absence of multimethod thermochronology, we cannot quantify these differences, but some amount of Cenozoic differential exhumation across the Ushba shear zone is likely required to generate these differences and field evidence (noted above) supports brittle slip along the Ushba shear zone (e.g., Lock & Willett, 2008). In Kazbegi, footwall ZHe analyses are not yet available to determine if the MCT shows a similar age offset.

Along the Kazbegi traverse, Miocene ZHe ages (~8–7 Ma) and Pliocene AHe ages (~3–2 Ma) produce thermal models indicating rapid cooling from at least 250 °C since ~9–8 Ma in both the granodiorite (K1) and MCT shear zone (K2), corresponding to at least ~8–10 km of exhumation, assuming a geothermal gradient of ~25–30 °C/km (Figures 6b and S9). Incorporating the ~96-Ma biotite $^{40}Ar/^{39}Ar$ total gas age into the thermal model for K1 suggests that Cenozoic cooling of the hanging wall prior to 10 Ma was relatively minor and that the Cenozoic temperature of sample K1 likely did not exceed ~300 °C (Figure 6b). This allows for a total of ~10–12 km of possible exhumation since ~10 Ma, assuming cooling from a maximum of ~300 °C to surface temperatures and a geothermal gradient of ~25–30 °C/km. We interpret the maximum temperature of ~300 °C, coupled with the $^{40}Ar/^{39}Ar$ ages of ~230-190 Ma from muscovite defining the foliation of the shear zone (K2; Figures 4g, 6a, and S5e), to indicate limited, if any, Late Cenozoic quartz-plastic deformation of the Gveleti shear zone.

The Kazbegi samples lie near the Pliocene to Quaternary volcanic center of Mt. Kazbegi (Figure 2; e.g., Lebedev et al., 2009, 2014, 2018), and magmatic activity could potentially affect low-temperature thermochronometric ages here via hydrothermal convection or a local increase in the geothermal gradient (e.g., Ehlers, 2005; Peyton & Carrapa, 2013). Our thermal modeling of sample K1 predicts cooling prior to onset of magmatism in this region at ~5 Ma (Figure 6b), and Pliocene AHe ages have been reported in other parts of the Greater Caucasus away from Cenozoic volcanic centers, including in the Tsei valley ~60 km northwest of Mt. Kazbegi (Figure 2; Avdeev & Niemi, 2011) and in the Svaneti region ~10 km south of the Dizi series (Figure 2b; Trexler, 2018). As a result, we infer, absent any clear indication to the contrary, that these ages represent tectonic exhumation rather than magmatic resetting. However, given the local prominence of Late Cenozoic magmatism, the geothermal gradient here may have been elevated relative to Svaneti, although we have no data to confirm or quantify this possibility. An elevated gradient of 40 °C/km, for example, would result in a maximum of ~8 km of exhumation in Kazbegi rather than the ~10–12 km estimated from 25–30 °C/km. Given this uncertainty, we take a conservative approach and use the estimate from Svaneti of at least ~5–8 km of exhumation exhumation of the MCT hanging wall since ~10 Ma.

5.5. Cenozoic Structures in the MCT Footwall

Results presented here and prior work combine to indicate significant Cenozoic cooling of the MCT footwall. Specifically, the Cenozoic ZHe ages in the Dizi series (N3) suggest Cenozoic cooling from temperatures >150 °C south of the MCT, and a previously reported ~2.5-Ma apatite fission track age from the southern margin of the Dizi series suggests very recent cooling of these rocks from at least ~115 °C (Figure 2;

Ketcham et al., 1999; Vincent et al., 2011). AHe ages of ~1–2 Ma in rocks farther to the south in Svaneti, as well as AHe ages of ~7–8 Ma in Kazbegi south of the MCT, provide additional evidence that a significant component of Cenozoic exhumation has been accommodated south of the MCT (Figure 2; Trexler, 2018). We interpret this Cenozoic exhumation south of the MCT to result from shortening on one or more additional major faults to the south. Notably, none of the MCT footwall rocks in this study exhibit the dynamic recrystallization seen in the hanging wall, leading us to conclude that quartz-plastic deformation in the MCT hanging wall is distinct from Late Cenozoic exhumation of both the MCT hanging wall and footwall (Figures 4c and 4d and 4h).

5.6. The Location of the MCT and Its Role in Arabia-Eurasia Collision

The usual definition of the MCT in the western Greater Caucasus is the thrust that places the crystalline basement in the range over sedimentary cover (e.g., Dotduyev, 1986; Mosar et al., 2010; Saintot, Brunet, et al., 2006; Zaridze, 1959). The presence of a north-dipping, greenschist-facies mylonitic shear zone at the contact between Paleozoic crystalline basement and Jurassic metasedimentary rocks on both the Svaneti and Kazbegi traverses (Figures 3 and 4) provides good reason to consider both the Ushba and Gveleti shear zones as part of the MCT. We see no geologic evidence to define faults to the south of the Gveleti shear zone as the MCT, as some studies do (e.g., Rogozhin et al., 2015; Vincent et al., 2018). Our data provide no new insight into the continuation of the MCT into the eastern Greater Caucasus, where no crystalline basement is exposed.

Given the evidence for important structures in the MCT footwall (this study; Mosar et al., 2010; Forte et al., 2010, 2013; Trexler, 2018), we speculate that the MCT may function as a backstop to a distributed system of faults in the footwall and largely exposes a record of older Paleozoic-Mesozoic tectonic events in the upper plate of the present collision. We infer that this distributed system of faults, including the MCT, merge at depth onto a single basal décollement carrying Greater Caucasus basement in its hanging wall. As a result, the surface expression of the MCT as a basement-involved thrust is connected to the Cenozoic basal décollement also called the MCT (e.g., Philip et al., 1989; Reilinger et al., 2006; Shempelev, 1978; Shempelev et al., 2017), but it is not the sole or primary structure accommodating Arabia-Eurasia convergence. Instead, deformation within the orogenic wedge of the Greater Caucasus is primarily confined to the foreland fold-thrust belt to the south, which enables the maintenance of critical taper, and the MCT backstop allows for continued growth of the wedge (Figure 1a).

6. Conclusions

New field observations, microstructural analysis, and geochronologic and thermochronologic data provide insight into basement-involved deformation along the MCT. The Greater Caucasus basement formed in the Early Paleozoic as a part of Gondwana, as indicated by zircon U-Pb age distributions comparable to those of modern rivers and microcontinents of Gondwanan affinity. We infer that this basement was then detached from Gondwana and subsequently accreted onto the Laurussian margin, likely during the Carboniferous, based on exhumation of high-pressure/temperature eclogite at ~330-300 Ma along an inferred suture on the northern flank of the Greater Caucasus (e.g., Philippot et al., 2001). This accretion resulted in amphibolite-facies low-pressure/temperature metamorphism and widespread granitoid plutonism throughout the basement, reflected in amphibolite-facies deformation textures and metamorphic and igneous zircon U-Pb ages of ~330-310 Ma.

Low-grade quartz-plastic deformation during Mesozoic back-arc rifting and inversion associated with development of the Caucasus Basin resulted in development of the MCT as an upper-crustal shear zone, as recorded by greenschist-facies deformation textures and Mesozoic mica $^{40}Ar/^{39}Ar$ ages. Our data suggest the shear zones formed at ~190 Ma along the Gveleti fault in Kazbegi and ~150–135 Ma along the Ushba thrust in Svaneti. These deformation textures suggest ~10–20 km of exhumation since that time, with thermal modeling of thermochronometric data predicting at least ~5–8 km since ~10 Ma in response to Cenozoic Arabia-Eurasia collision. An approximately 11 Ma difference in Cenozoic zircon (U-Th)/He ages across the MCT in Svaneti suggests that the MCT may have been reactivated as a brittle structure during Arabia-Eurasia collision, but it likely serves as the backstop to the orogen and is only one of several structures accommodating Arabia-Eurasia convergence.

Acknowledgments

This material is based upon work supported by the National Science Foundation under grant 0810285 and 1524631 to E. Cowgill and 0810067 and 1524304 to N. Niemi from the EAR-Tectonics program, with support from the Office of International Science and Engineering. Additional funding for this project was provided by small grants to D. Vasey from the Geological Society of America Graduate Student Research Grants, Sigma Xi Grants-in-Aid of Research, and the UC Davis Durrell Fund. Reviews from Nadine McQuarrie and an anonymous reviewer greatly improved the quality of this manuscript. We thank G. Gehrels, M. Pecha, D. Giesler, and K. Plange for assistance at the Arizona LaserChron Center, supported by NSF-EAR grant 1649254, M. Grove and T. O'Brien at the Stanford University Noble Gas Lab for $^{40}Ar/^{39}Ar$ analyses, A. Maslyn at the University of Michigan Thermochronology Lab for (U-Th)/He analyses, and G. Baxter at UC Davis for preparing thin sections. We also thank A. Okrostsvaridze, Z. Javakhishvili, E. Young, G. Boichenko, and D. Akubardia for field assistance and A. Forte and C. Trexler for sharing samples. Additional analytical methods, figures, data tables, and QTQt input files are available in the supporting information, as well as in the repository Dryad (Vasey et al., 2020) at https://doi.org/10.25338/B8D61N.

References

Adamia, S., Akhvlediani, K. T., Kilasonia, V. M., Nairn, A. E. M., Papava, D., & Patton, D. K. (1992). Geology of the Republic of Georgia: A Review. *International Geology Review*, *34*, 447–476. https://doi.org/10.1080/00206819209465614

Adamia, S., Alania, V., Chabukiani, A., Kutelia, Z., & Sadradze, N. (2011). Great Caucasus (Cavcasioni): A long-lived north-Tethyan back-arc basin. *Turkish Journal of Earth Sciences*, *20*, 611–628.

Adamia, S. A., Lordkipanidze, M., & Zakariadze, G. S. (1977). Evolution of an active continental margin as exemplified by the Alpine history of the Caucasus. *Tectonophysics*, *40*, 183–199.

Agard, P., Omrani, J., Jolivet, L., & Mouthereau, F. (2005). Convergence history across Zagros (Iran): Constraints from collisional and earlier deformation. *International Journal of Earth Sciences*, *94*, 401–419. https://doi.org/10.1007/s00531-005-0481-4

Alavi, M. (1991). Sedimentary and structural characteristics of the Paleo-Tethys remnants in northeastern Iran. *GSA Bulletin*, *103*, 983–992. https://doi.org/10.1130/0016-7606(1991)103<0983:SASCOT>2.3.CO;2

Alexandrov, P., Ruffet, G., & Cheilletz, A. (2002). Muscovite recrystallization and saddle-shaped $^{40}Ar/^{39}Ar$ age spectra: Example from the Blond granite (Massif Central, France). *Geochimica et Cosmochimica Acta*, *66*, 1793–1807. https://doi.org/10.1016/S0016-7037(01)00895-X

Allen, M. B., Morton, A. C., Fanning, C. M., Ismail-Zadeh, A. J., & Kroonenberg, S. B. (2006). Zircon age constraints on sediment provenance in the Caspian region. *Journal of the Geological Society, London*, *163*, 647–655. https://doi.org/10.1144/0016-764920-068

Allmendinger, R. W., Cardozo, N., & Fisher, D. M. (2011). *Structural geology algorithms: Vectors and tensors*. Cambridge, UK: Cambridge University Press.

Avdeev, B., 2011, Tectonics of the Greater Caucasus and the Arabia-Eurasia orogen [PhD thesis]: University of Michigan, 137 p.

Avdeev, B., & Niemi, N. A. (2011). Rapid Pliocene exhumation of the central Greater Caucasus constrained by low-temperature thermochronometry. *Tectonics*, *30*, TC2009. https://doi.org/10.1029/2010TC002808

Avrahamov, K.P., Kipiani, Ya.R., and Shirayan, E.V., 1983, Geological Map of the Georgian SSR, sheet K-38-42-V, scale 1:50,000: USSR Ministry of Geology, Leningrad.

Bahlburg, H., Vervoort, J. D., & DuFrane, S. A. (2010). Plate tectonic significance of Middle Cambrian and Ordovician siliciclastic rocks of the Bavarian Facies, Armorican Terrane Assemblage, Germany - U-Pb and Hf isotope evidence from detrital zircons. *Gondwana Research*, *17*, 223–235. https://doi.org/10.1016/j.gr.2009.11.007

Bailey, J. E., & Hirsch, P. B. (1962). The recrystallization process in some polycrystalline metals. *Proc. R. Soc. Lond. A*, *267*, 11–30. https://doi.org/10.1098/rspa.1962.0080

Banks, C. J., Robinson, A. G., & Williams, M. P. (1997). Structure and regional tectonics of the Achara-Trialet fold belt and the adjacent Rioni and Kartli foreland basins, Republic of Georgia. In A. G. Robinson (Ed.), *Regional and Petroleum Geology of the Black Sea and Surrounding Region*, (pp. 331–346). Tulsa, OK: American Association of Petroleum Geologists.

Bellanger, M., Bellahsen, N., Jolivet, L., Baudin, T., Augier, R., and Boutoux, A. (2014). Basement shear zones development and shortening kinematics in the Ecrins Massif, Western Alps: *Tectonics*, *33*, 2013TC003294. https://doi.org/10.1002/2013TC003294

Benson, T. R., Mahood, G. A., & Grove, M. (2017). Geology and $^{40}Ar/^{39}Ar$ geochronology of the middle Miocene McDermitt volcanic field, Oregon and Nevada: Silicic volcanism associated with propagating flood basalt dikes at initiation of the Yellowstone hotspot. *GSA Bulletin*, *129*, 1027–1051. https://doi.org/10.1130/B31642.1

Byrne, D. E., Wang, W., & Davis, D. M. (1993). Mechanical role of backstops in the growth of forearcs. *Tectonics*, *12*, 123–144. https://doi.org/10.1029/92TC00618

Cardozo, N., & Allmendinger, R. W. (2013). Spherical projections with OSXStereonet. *Computers & Geosciences*, *51*, 193–205. https://doi.org/10.1016/j.cageo.2012.07.021

Chapple, W. M. (1978). Mechanics of thin-skinned fold-and-thrust belts. *GSA Bulletin*, *89*, 1189–1198. https://doi.org/10.1130/0016-7606(1978)89<1189:MOTFB>2.0.CO;2

Cheilletz, A., Ruffet, G., Marignac, C., Kolli, O., Gasquet, D., Féraud, G., & Bouillin, J. P. (1999). $^{40}Ar/^{39}Ar$ dating of shear zones in the Variscan basement of Greater Kabylia (Algeria). Evidence of an Eo-Alpine event at 128 Ma (Hauterivian–Barremian boundary): geodynamic consequences. *Tectonophysics*, *306*, 97–116. https://doi.org/10.1016/S0040-1951(99)00047-5

Coble, M. A., Grove, M., & Calvert, A. T. (2011). Calibration of Nu-Instruments Noblesse multicollector mass spectrometers for argon isotopic measurements using a newly developed reference gas. *Chemical Geology*, *290*, 75–87. https://doi.org/10.1016/j.chemgeo.2011.09.003

Cowgill, E., Forte, A. M., Niemi, N., Avdeev, B., Tye, A., Trexler, C., et al. (2016). Relict basin closure and crustal shortening budgets during continental collision: An example from Caucasus sediment provenance. *Tectonics*, *35*, 2918–2947. https://doi.org/10.1002/2016TC004295

Cowgill, E., Niemi, N. A., Forte, A. M., & Trexler, C. C. (2018). Reply to comment by Vincent et al. *Tectonics*, *37*, 1017–1028. https://doi.org/10.1002/2017TC004793

Dahlen, F. A. (1984). Noncohesive critical Coulomb wedges: An exact solution. *Journal of Geophysical Research: Solid Earth*, *89*, 10,125–10,133. https://doi.org/10.1029/JB089iB12p10125

Dalrymple, B. G., & Lanphere, M. A. (1974). $^{40}Ar/^{39}Ar$ age spectra of some undisturbed terrestrial samples. *Geochimica et Cosmochimica Acta*, *38*, 715–738. https://doi.org/10.1016/0016-7037(74)90146-X

Davis, D., Suppe, J., & Dahlen, F. A. (1983). Mechanics of fold-and-thrust belts and accretionary wedges. *Journal of Geophysical Research: Solid Earth*, *88*, 1153–1172. https://doi.org/10.1029/JB088iB02p01153

Dickinson, W. R., & Gehrels, G. E. (2009). Use of U-Pb ages of detrital zircons to infer maximum depositional ages of strata: A test against a Colorado Plateau Mesozoic database. *Earth and Planetary Science Letters*, *288*, 115–125. https://doi.org/10.1016/j.epsl.2009.09.013

Dotduyev, S. (1986). Nappe structure of the Greater Caucasus range. *Geotectonics*, *20*, 420–430.

Drost, K., Gerdes, A., Jeffries, T., Linnemann, U., & Storey, C. (2011). Provenance of Neoproterozoic and early Paleozoic siliciclastic rocks of the Teplá-Barrandian unit (Bohemian Massif): Evidence from U-Pb detrital zircon ages. *Gondwana Research*, *19*, 213–231. https://doi.org/10.1016/j.gr.2010.05.003

Egan, S. S., Mosar, J., Brunet, M.-F., & Kangarli, T. (2009). Subsidence and uplift mechanisms within the South Caspian Basin: Insights from the onshore and offshore Azerbaijan region. *Geological Society, London, Special Publications*, *312*, 219–240. https://doi.org/10.1144/SP312.11

Ehlers, T. A. (2005). Crustal thermal processes and the interpretation of thermochronometer data. *Reviews in Mineralogy and Geochemistry*, *58*, 315–350. https://doi.org/10.2138/rmg.2005.58.12

Ershov, A. V., Brunet, M.-F., Nikishin, A. M., Bolotov, S. N., Nazarevich, B. P., & Korotaev, M. V. (2003). Northern Caucasus basin: Thermal history and synthesis of subsidence models. *Sedimentary Geology*, *156*, 95–118. https://doi.org/10.1016/S0037-0738(02)00284-1

Farley, K. A. (2000). Helium diffusion from apatite: General behavior as illustrated by Durango fluorapatite. *Journal of Geophysical Research*, *105*, 2903–2914.

Farley, K. A., Wolf, R. A., & Silver, L. T. (1996). The effects of long alpha-stopping distances on (U-Th)/He ages. *Geochimica et Cosmochimica Acta*, *60*, 4223–4229. https://doi.org/10.1016/S0016-7037(96)00193-7

Flowers, R. M., Ketcham, R. A., Shuster, D. L., & Farley, K. A. (2009). Apatite (U–Th)/He thermochronometry using a radiation damage accumulation and annealing model. *Geochimica et Cosmochimica Acta*, *73*, 2347–2365. https://doi.org/10.1016/j.gca.2009.01.015

Forte, A. M., Cowgill, E., Bernardin, T., Kreylos, O., & Hamann, B. (2010). Late Cenozoic deformation of the Kura fold-thrust belt, southern Greater Caucasus. *Geological Society of America Bulletin*, *122*, 465–486. https://doi.org/10.1130/B26464.1

Forte, A. M., Cowgill, E., Murtuzayev, I., Kangarli, T., & Stoica, M. (2013). Structual geometries and magnitude of shortening in the eastern Kura fold-thrust belt, Azerbaijan: Implications for the development of the Greater Caucasus Mountains. *Tectonics*, *32*. https://doi.org/10.1002/tect.20032

Forte, A. M., Cowgill, E., & Whipple, K. X. (2014). Transition from a singly vergent to doubly vergent wedge in a young orogen: The Greater Caucasus: *Tectonics*, *33*, 2014TC003651. https://doi.org/10.1002/2014TC003651

Forte, A. M., Whipple, K. X., & Cowgill, E. (2015). Drainage network reveals patterns and history of active deformation in the eastern Greater Caucasus. *Geosphere*, *11*, 1343–1364. https://doi.org/10.1130/GES01121.1

Gallagher, K. (2012). Transdimensional inverse thermal history modeling for quantitative thermochronology. *Journal of Geophysical Research: Solid Earth*, *117*, B02408. https://doi.org/10.1029/2011JB008825

Gamkrelidze, I., Shengelia, D., Tsutsunava, T., Chung, S. L., Yichiu, H., & Chikhelidze, K. (2011). New date on the U-Pb zircon age of the pre-Alpine crystalline basement of the Black-Sea-central Transcaucasian Terrane and their geological significance. *Bulletin of the Georgian National Academy of Sciences*, *5*, 64–76.

Gamkrelidze, I. P. (1986). Geodynamic evolution of the Caucasus and adjacent areas in Alpine time. *Tectonophysics*, *127*, 261–277. https://doi.org/10.1016/0040-1951(86)90064-8

Gamkrelidze, P.D., and Kakhazdze, I.R., 1959, Geological Map of the USSR, Caucasus series sheet K-38-VII, scale 1:200,000: Ministry of Geology and Mineral Protection USSR, Moscow.

Geguchadze, Sh.H., Gvineria, L.C., Kalinin, E.V., and Beradze, R.P., 1985, Geological Map of the Georgian SSR, sheet K-38-25-V, scale 1:50,000: USSR Ministry of Geology, Leningrad.

Gehrels, G., & Pecha, M. (2014). Detrital zircon U-Pb geochronology and Hf isotope geochemistry of Paleozoic and Triassic passive margin strata of western North America. *Geosphere*, *10*, 49–65. https://doi.org/10.1130/GES00889.1

Gehrels, G., Valencia, V., & Pullen, A. (2006). Detrital zircon geochronology by laser-ablation multicollector ICPMS at the Arizona LaserChron Center. *The Paleontological Society Papers*, *12*, 67–76. https://doi.org/10.1017/S1089332600001352

Gehrels, G. E., Valencia, V. A., & Ruiz, J. (2008). Enhanced precision, accuracy, efficiency, and spatial resolution of U-Pb ages by laser ablation–multicollector–inductively coupled plasma–mass spectrometry: Geochemistry. *Geophysics, Geosystems*, *9*, Q03017. https://doi.org/10.1029/2007GC001805

Granado, P., Ferrer, O., Muñoz, J. A., Thöny, W., & Strauss, P. (2017). Basin inversion in tectonic wedges: Insights from analogue modelling and the Alpine-Carpathian fold-and-thrust belt. *Tectonophysics*, *703–704*, 50–68. https://doi.org/10.1016/j.tecto.2017.02.022

Grove, M., & Harrison, T. M. (1996). ^{40}Ar* diffusion in Fe-rich biotite. *American Mineralogist*, *81*, 940–951. https://doi.org/10.2138/am-1996-7-816

Gubkina, A.N., and Ermakov, V.A., 1989, Geological Map of the USSR, Caucasus series sheet K-38-IX, scale 1:200,000: USSR Ministry of Geology, Leningrad.

Guenthner, W. R., Reiners, P. W., Ketcham, R. A., Nasdala, L., & Giester, G. (2013). Helium diffusion in natural zircon: Radiation damage, anisotropy, and the interpretation of zircon (U-Th)/He thermochronology. *American Journal of Science*, *313*, 145–198. https://doi.org/10.2475/03.2013.01

Hanel, M., Gurbanov, A., & Lippolt, H. (1992). Age and genesis of granitoids from the Main-Range and Bechasyn zones of the western Great Caucasus. *Neues Jahrbuch fur Mineralogie Monatshefte*, *12*, 529–529.

Harrison, T. M., Célérier, J., Aikman, A. B., Hermann, J., & Heizler, M. T. (2009). Diffusion of ^{40}Ar in muscovite. *Geochimica et Cosmochimica Acta*, *73*, 1039–1051. https://doi.org/10.1016/j.gca.2008.09.038

Hempton, M. R. (1985). Structure and deformation history of the Bitlis suture near Lake Hazar, southeastern Turkey. *GSA Bulletin*, *96*, 233–243. https://doi.org/10.1130/0016-7606(1985)96<233:SADHOT>2.0.CO;2

Hirth, G., & Tullis, J. (1992). Dislocation creep regimes in quartz aggregates. *Journal of Structural Geology*, *14*, 145–159.

Holdaway, M. J., & Lee, S. M. (1977). Fe-Mg cordierite stability in high-grade pelitic rocks based on experimental, theoretical, and natural observations. *Contributions to Mineralogy and Petrology*, *63*, 175–198. https://doi.org/10.1007/BF00398778

Iizuka, T., Campbell, I. H., Allen, C. M., Gill, J. B., Maruyama, S., & Makoka, F. (2013). Evolution of the African continental crust as recorded by U–Pb, Lu–Hf and O isotopes in detrital zircons from modern rivers. *Geochimica et Cosmochimica Acta*, *107*, 96–120. https://doi.org/10.1016/j.gca.2012.12.028

Jackson, J. (1992). Partitioning of strike-slip and convergent motion between Eurasia and Arabia in eastern Turkey and the Caucasus. *Journal of Geophysical Research: Solid Earth*, *97*, 12,471–12,479. https://doi.org/10.1029/92JB00944

Kalvoda, J., & Bábek, O. (2010). The margins of Laurussia in central and southeast Europe and southwest Asia. *Gondwana Research*, *17*, 526–545. https://doi.org/10.1016/j.gr.2009.09.012

Kamzolkin, V. A., Somin, M. L., Latyshev, A. V., Vidyapin, Y. P., & Ivanov, S. D. (2019). The Late Vendian Basement within the Limits of the Blyb Metamorphic Complex, Peredovoi Range of the Greater Caucasus. *Doklady Earth Sciences*, *487*(2), 877–880. https://doi.org/10.1134/s1028334x19080038

Kapp, P., Yin, A., Manning, C. E., Harrison, T. M., Taylor, M. H., & Ding, L. (2003). Tectonic evolution of the early Mesozoic blueschist-bearing Qiangtang metamorphic belt, central Tibet. *Tectonics*, *22*. https://doi.org/10.1029/2002TC001383

Kelley, S. (2002). Excess argon in K–Ar and Ar–Ar geochronology. *Chemical Geology*, *188*, 1–22. https://doi.org/10.1016/S0009-2541(02)00064-5

Ketcham, R. A., Donelick, R. A., & Carlson, W. D. (1999). Variability of apatite fission-track annealing kinetics: III. Extrapolation to geological time scales. *American Mineralogist*, *84*, 1235–1255. https://doi.org/10.2138/am-1999-0903

Ketcham, R. A., Gautheron, C., & Tassan-Got, L. (2011). Accounting for long alpha-particle stopping distances in (U–Th–Sm)/He geochronology: Refinement of the baseline case. *Geochimica et Cosmochimica Acta*, *75*, 7779–7791. https://doi.org/10.1016/j.gca.2011.10.011

Khain, V. E., Gadjiev, A. N., & Kengerli, T. N. (2007). Tectonic origin of the Apsheron Threshold in the Caspian Sea. *Doklady Earth Sciences*, *414*(1), 552–556. https://doi.org/10.1134/S1028334X07040149

Kopp, M. L., & Shcherba, I. G. (1985). Late alpine development of the east Caucasus. *Geotectonics*, *19*, 497–507.

Lacombe, O., & Bellahsen, N. (2016). Thick-skinned tectonics and basement-involved fold–thrust belts: Insights from selected Cenozoic orogens. *Geological Magazine*, *153*, 763–810. https://doi.org/10.1017/S0016756816000078

Lacombe, O., & Mouthereau, F. (2002). Basement-involved shortening and deep detachment tectonics in forelands of orogens: Insights from recent collision belts (Taiwan, Western Alps, Pyrenees). *Tectonics*, *21*, 12–11. https://doi.org/10.1029/2001TC901018

Lebedev, V. A., Bubnov, S. N., Chernyshev, I. V., Chugaev, A. V., Goltzman, Y. V., Vashakidze, G. T., & Bairova, E. D. (2009). Geochronology and genesis of the young (Pliocene) granitoids of the Greater Caucasus: Dzhimara multiphase Massif of the Kazbek neovolcanic area. *Geochemistry International*, *47*(6), 550–567. https://doi.org/10.1134/S0016702909060020

Lebedev, V. A., Parfenov, A. V., Vashakidze, G. T., Chernyshev, I. V., & Gabarashvili, Q. A. (2014). Major events in evolution of the Kazbek neovolcanic center, Greater Caucasus: Isotope-geochronological data. *Doklady Earth Sciences*, *458*(1), 1092–1098. https://doi.org/10.1134/S1028334X14090074

Lebedev, V. A., Parfenov, A. V., Vashakidze, G. T., Gabarashvili, Q. A., Chernyshev, I. V., & Togonidze, M. G. (2018). Chronology of magmatic activity and petrologic–mineralogical characteristics of lavas of Kazbek Quaternary volcano, Greater Caucasus. *Petrology*, *26*(1), 1–28. https://doi.org/10.1134/S086959111801006X

Leonov, Y. G. (1967). Tectonics of the Lower-Middle Jurassic sediments in the eastern part of the central Caucasus. *Geotectonics*, *3*, 152–159.

Leonov, Y. G. (1969). The Early and Middle Jurassic phases of uplift and folding in the Greater Caucasus. *Geotectonics*, *6*, 380–383.

Linnemann, U., Pereira, F., Jeffries, T. E., Drost, K., & Gerdes, A. (2008). The Cadomian Orogeny and the opening of the Rheic Ocean: The diacrony of geotectonic processes constrained by LA-ICP-MS U–Pb zircon dating (Ossa-Morena and Saxo-Thuringian Zones, Iberian and Bohemian Massifs). *Tectonophysics*, *461*, 21–43. https://doi.org/10.1016/j.tecto.2008.05.002

Lock, J., & Willett, S. (2008). Low-temperature thermochronometric ages in fold-and-thrust belts. *Tectonophysics*, *456*, 147–162. https://doi.org/10.1016/j.tecto.2008.03.007

Ludwig, K. (2008). Isoplot 3.7: Berkeley Geochronology Center Special Publication *4*, 77 p.

Matte, P. (2001). The Variscan collage and orogeny (480–290 Ma) and the tectonic definition of the Armorica microplate: A review. *Terra Nova*, *13*, 122–128. https://doi.org/10.1046/j.1365-3121.2001.00327.x

Mayringer, F., Treloar, P. J., Gerdes, A., Finger, F., & Shengelia, D. (2011). New age data from the Dzirula Massif, Georgia: Implications for the evolution of the Caucasian Variscides. *American Journal of Science*, *311*, 404–441. https://doi.org/10.2475/05.2011.02

McDougall, I., & Harrison, T. M. (1999). *Geochronology and thermochronology by the $^{40}Ar/^{39}Ar$ Method*. Oxford, UK: Oxford University Press.

McQuarrie, N. (2002). The kinematic history of the central Andean fold-thrust belt, Bolivia: Implications for building a high plateau. *GSA Bulletin*, *114*, 950–963. https://doi.org/10.1130/0016-7606(2002)114<0950:TKHOTC>2.0.CO;2

McQuarrie, N., & van Hinsbergen, D. J. J. (2013). Retrodeforming the Arabia-Eurasia collision zone: Age of collision versus magnitude of continental subduction. *Geology*, *41*, 315–318. https://doi.org/10.1130/Gs33591.1

Metcalfe, I. (2013). Gondwana dispersion and Asian accretion: Tectonic and palaeogeographic evolution of eastern Tethys. *Journal of Asian Earth Sciences*, *66*, 1–33. https://doi.org/10.1016/j.jseaes.2012.12.020

Mirnejad, H., Lalonde, A. E., Obeid, M., & Hassanzadeh, J. (2013). Geochemistry and petrogenesis of Mashhad granitoids: An insight into the geodynamic history of the Paleo-Tethys in northeast of Iran. *Lithos*, *170–171*, 105–116. https://doi.org/10.1016/j.lithos.2013.03.003

Mitchell, J., & Westaway, R. (1999). Chronology of Neogene and Quaternary uplift and magmatism in the Caucasus: Constraints from K–Ar dating of volcanism in Armenia. *Tectonophysics*, *304*, 157–186. https://doi.org/10.1016/S0040-1951(99)00027-X

Mosar, J., Kangarli, T., Bochud, M., Glasmacher, U. A., Rast, A., Brunet, M.-F., & Sosson, M. (2010). Cenozoic-Recent tectonics and uplift in the Greater Caucasus: A perspective from Azerbaijan. *Geological Society, London, Special Publications*, *340*, 261–280. https://doi.org/10.1144/SP340.12

Nalivkin, D.V., 1976, Geologic Map of the Caucasus: Ministry of Geology, USSR.

Nance, R. D., Gutiérrez-Alonso, G., Keppie, J. D., Linnemann, U., Murphy, J. B., Quesada, C., et al. (2010). Evolution of the Rheic Ocean. *Gondwana Research*, *17*, 194–222. https://doi.org/10.1016/j.gr.2009.08.001

Natal'in, B. A., & Şengör, A. M. C. (2005). Late Palaeozoic to Triassic evolution of the Turan and Scythian platforms: The pre-history of the Palaeo-Tethyan closure. *Tectonophysics*, *404*, 175–202. https://doi.org/10.1016/j.tecto.2005.04.011

Niemi, N. A., & Clark, M. K. (2018). Long-term exhumation rates exceed paleoseismic slip rates in the central Santa Monica Mountains, Los Angeles County, California. *Geology*, *46*, 63–66. https://doi.org/10.1130/G39388.1

Nikishin, A., Ziegler, P., Bolotov, S., & Fokin, P. (2011). Late Palaeozoic to Cenozoic evolution of the Black Sea-Southern Eastern Europe region: A view from the Russian Platform. *Turkish Journal of Earth Sciences*, *20*, 571–634.

Okay, A. I., Bozkurt, E., Satır, M., Yiğitbaş, E., Crowley, Q. G., & Shang, C. K. (2008). Defining the southern margin of Avalonia in the Pontides: Geochronological data from the Late Proterozoic and Ordovician granitoids from NW Turkey. *Tectonophysics*, *461*, 252–264. https://doi.org/10.1016/j.tecto.2008.02.004

Okay, A. I., & Topuz, G. (2016). Variscan orogeny in the Black Sea region. *International Journal of Earth Sciences*, *106*(2), 569–592. https://doi.org/10.1007/s00531-016-1395-z

Okay, A. I., Zattin, M., & Cavazza, W. (2010). Apatite fission-track data for the Miocene Arabia-Eurasia collision. *Geology*, *38*, 35–38. https://doi.org/10.1130/G30234.1

Pavlenkova, G. A. (2012). Crustal structure of the Caucasus from the Stepnoe-Bakuriani and Volgograd-Nakhichevan DSS profiles (reinterpretation of the primary data). *Izvestiya, Physics of the Solid Earth*, *48*, 375–384. https://doi.org/10.1134/S1069351312040040

Perchuk, A., & Philippot, P. (1997). Rapid cooling and exhumation of eclogitic rocks from the great Caucasus, Russia. *Journal of Metamorphic Geology*, *15*, 299–310.

Peyton, S.L., and Carrapa, B. (2013). An introduction to low-temperature thermochronologic techniques, methodology, and applications, p. 15–36, https://doi.org/10.1306/13381688St653578.

Pfiffner, O. A. (2006). Thick-skinned and thin-skinned styles of continental contraction. *Geological Society of America Special Papers*, *414*, 153–177. https://doi.org/10.1130/2006.2414(09)

Philip, H., Cisternas, A., Gvishiani, A., & Gorshkov, A. (1989). The Caucasus: An actual example of the initial stages of continental collision. *Tectonophysics*, *161*, 1–21. https://doi.org/10.1016/0040-1951(89)90297-7

Philippot, P., Blichert-Toft, J., Perchuk, A., Costa, S., & Gerasimov, V. (2001). Lu–Hf and Ar–Ar chronometry supports extreme rate of subduction zone metamorphism deduced from geospeedometry. *Tectonophysics*, *342*, 23–38. https://doi.org/10.1016/S0040-1951(01)00155-X

Pryer, L. L. (1993). Microstructures in feldspars from a major crustal thrust zone: The Grenville Front, Ontario, Canada. *Journal of Structural Geology*, *15*, 21–36.
Pullen, A., Ibáñez-Mejía, M., Gehrels, G. E., Ibáñez-Mejía, J. C., & Pecha, M. (2014). What happens when n = 1000? Creating large-n geochronological datasets with LA-ICP-MS for geologic investigations. *Journal of Analytical Atomic Spectrometry*, *29*, 971–980. https://doi.org/10.1039/C4JA00024B
Pullen, A., Kapp, P., Gehrels, G. E., Vervoort, J. D., & Ding, L. (2008). Triassic continental subduction in central Tibet and Mediterranean-style closure of the Paleo-Tethys Ocean. *Geology*, *36*, 351–354. https://doi.org/10.1130/G24435A.1
Reilinger, R., McClusky, S., Vernant, P., Lawrence, S., Ergintav, S., Cakmak, R., et al. (2006). GPS constraints on continental deformation in the Africa-Arabia-Eurasia continental collision zone and implications for the dynamics of plate interactions. *Journal of Geophysical Research: Solid Earth*, *111*, B05411. https://doi.org/10.1029/2005JB004051
Reiners, P. W., & Brandon, M. T. (2006). Using thermochronology to understand orogenic erosion. *Annu. Rev. Earth Planet. Sci.*, *34*, 419–466.
Reiners, P.W., and Nicolescu, S., 2006, Measurement of parent nuclides for (U-Th)/He chronomtry by solution sector ICP-MS: Arizona Radiogenic Helium Dating Laboratory, 33 p., http://www.geo.arizona.edu/~reiners/arhdl/arhdlrep1.pdf.
Reiners, P. W., Spell, T. L., Nicolescu, S., & Zanetti, K. A. (2004). Zircon (U-Th)/He thermochronometry: He diffusion and comparisons with 40Ar/39Ar dating. *Geochimica et Cosmochimica Acta*, *68*, 1857–1887. https://doi.org/10.1016/j.gca.2003.10.021
Rogozhin, E. A., Gorbatikov, A. V., Stepanova, M. Y., Ovsyuchenko, A. N., Andreeva, N. V., & Kharazova, Y. V. (2015). The structural framework and recent geodynamics of the Greater Caucasus Meganticlinorium in the light of new data on its deep structure. *Geotectonics*, *49*(2), 123–134. https://doi.org/10.1134/S0016852115020053
Rolland, Y., Hässig, M., Bosch, D., Meijers, M. J. M., Sosson, M., Bruguier, O., et al. (2016). A review of the plate convergence history of the East Anatolia-Transcaucasus region during the Variscan: Insights from the Georgian basement and its connection to the Eastern Pontides. *Journal of Geodynamics*, *96*, 131–145. https://doi.org/10.1016/j.jog.2016.03.003
Rolland, Y., Sosson, M., Adamia, S., & Sadradze, N. (2011). Prolonged Variscan to Alpine history of an active Eurasian margin (Georgia, Armenia) revealed by $^{40}Ar/^{39}Ar$ dating. *Gondwana Research*, *20*, 798–815. https://doi.org/10.1016/j.gr.2011.05.007
Rossetti, F., Faccenna, C., & Ranalli, G. (2002). The influence of backstop dip and convergence velocity in the growth of viscous doubly-vergent orogenic wedges: insights from thermomechanical laboratory experiments. *Journal of Structural Geology*, *24*, 953–962. https://doi.org/10.1016/S0191-8141(01)00127-4
Ruban, D. A. (2007). Jurassic transgressions and regressions in the Caucasus (northern Neotethys Ocean) and their influences on the marine biodiversity. *Palaeogeography, Palaeoclimatology, Palaeoecology*, *251*, 422–436. https://doi.org/10.1016/j.palaeo.2007.04.008
Ruban, D. A., Zerfass, H., & Yang, W. (2007). A new hypothesis on the position of the Greater Caucasus Terrane in the Late Palaeozoic-Early Mesozoic based on palaeontologic and lithologic data. *Trabajos de Geología*, *27*, 19–27.
Rubatto, D. (2017). Zircon: The metamorphic mineral. *Reviews in Mineralogy and Geochemistry*, *83*, 261–295. https://doi.org/10.2138/rmg.2017.83.9
Rubatto, D., Hermann, J., Berger, A., & Engi, M. (2009). Protracted fluid-induced melting during Barrovian metamorphism in the Central Alps. *Contributions to Mineralogy and Petrology*, *158*, 703–722. https://doi.org/10.1007/s00410-009-0406-5
Safonova, I., Maruyama, S., Hirata, T., Kon, Y., & Rino, S. (2010). LA ICP MS U-Pb ages of detrital zircons from Russia largest rivers: Implications for major granitoid events in Eurasia and global episodes of supercontinent formation. *Journal of Geodynamics*, *50*, 134–153. https://doi.org/10.1016/j.jog.2010.02.008
Saintot, A., Brunet, M.-F., Yakovlev, F., Sébrier, M., Stephenson, R., Ershov, A., et al. (2006). The Mesozoic-Cenozoic tectonic evolution of the Greater Caucasus. *Geological Society, London, Memoirs*, *32*, 277–289. https://doi.org/10.1144/GSL.MEM.2006.032.01.16
Saintot, A., Stephenson, R. A., Stovba, S., Brunet, M.-F., Yegorova, T., & Starostenko, V. (2006). The evolution of the southern margin of Eastern Europe (Eastern European and Scythian platforms) from the Latest Precambrian-Early Palaeozoic to the Early Cretaceous. *Geological Society, London, Memoirs*, *32*, 481–505. https://doi.org/10.1144/GSL.MEM.2006.032.01.30
Şengör, A. M. C. (1979). Mid-Mesozoic closure of Permo–Triassic Tethys and its implications. *Nature*, *279*, 590–593. https://doi.org/10.1038/279590a0
Şengör, A. M. C. (2013). Outcrops, isotopic ages, terranes and the undesirable fate of tectonic interpretations. *Geodinamica Acta*, *26*, 159–174. https://doi.org/10.1080/09853111.2013.858953
Shaw, J., Gutiérrez-Alonso, G., Johnston, S. T., & Galán, D. P. (2014). Provenance variability along the Early Ordovician north Gondwana margin: Paleogeographic and tectonic implications of U-Pb detrital zircon ages from the Armorican Quartzite of the Iberian Variscan belt. *Geological Society of America Bulletin*, *126*, 702–719. https://doi.org/10.1130/B30935.1
Shempelev, A. G. (1978). Deep expression of the Main Caucasian Overthrust. *Geotectonics*, *12*, 437–443.
Shempelev, A. G., Zaalishvili, V. B., & Kukhmazov, S. U. (2017). Deep structure of the western part of the Central Caucasus from geophysical data. *Geotectonics*, *51*(5), 479–488. https://doi.org/10.1134/S0016852117050053
Shengelia, D., Tsutsunava, T., Chichinadze, G., & Beridze, G. (2014). Some questions on structure, Variscan regional metamorphism and granitoid magmatism of the Caucasian Terrane Crystallinicum. *Bulletin of the Georgian National Academy of Sciences*, *8*, 56–63.
Sokhadze, G., Floyd, M., Godoladze, T., King, R., Cowgill, E. S., Javakhishvili, Z., et al. (2018). Active convergence between the Lesser and Greater Caucasus in Georgia: Constraints on the tectonic evolution of the Lesser–Greater Caucasus continental collision. *Earth and Planetary Science Letters*, *481*, 154–161. https://doi.org/10.1016/j.epsl.2017.10.007
Somin, M. (2000). Structure of axial zones in the Central Caucasus. *Doklady Earth Sciences*, *375*, 1371–1374.
Somin, M. L. (2011). Pre-Jurassic basement of the Greater Caucasus: Brief overview. *Turkish Journal of Earth Sciences*, *20*, 545–610.
Somin, M. L., Kotov, A. B., Sal'nikova, E. B., Levchenkov, O. A., Pis'mennyi, A. N., & Yakovleva, S. Z. (2006). Paleozoic rocks in infrastructure of the metamorphic core, the Greater Caucasus Main Range zone. *Stratigraphy and Geological Correlation*, *14*(5), 475–485. https://doi.org/10.1134/S0869593806050029
Sosson, M., Stephenson, R., Sheremet, Y., Rolland, Y., Adamia, S., Melkonian, R., et al. (2016). The eastern Black Sea-Caucasus region during the Cretaceous: New evidence to constrain its tectonic evolution. *Comptes Rendus Geoscience*, *348*, 23–32. https://doi.org/10.1016/j.crte.2015.11.002
Spear, F. S., & Cheney, J. T. (1989). A petrogenetic grid for pelitic schists in the system SiO2-Al2O3-FeO-MgO-K2O-H2O. *Contributions to Mineralogy and Petrology*, *101*, 149–164. https://doi.org/10.1007/BF00375302
Stampfli, G. M. (2013). Response to the comments on "The formation of Pangea" by D.A. Ruban. *Tectonophysics*, *608*, 1445–1447. https://doi.org/10.1016/j.tecto.2013.09.004
Stampfli, G. M., Hochard, C., Vérard, C., Wilhem, C., & von Raumer, J. (2013). The formation of Pangea. *Tectonophysics*, *593*, 1–19. https://doi.org/10.1016/j.tecto.2013.02.037

Stipp, M., Stünitz, H., Heilbronner, R., & Schmid, S. M. (2002a). Dynamic recrystallization of quartz: Correlation between natural and experimental conditions. *Geological society, London, Special Publications*, *200*, 171–190. https://doi.org/10.1144/GSL.SP.2001.200.01.11

Stipp, M., Stünitz, H., Heilbronner, R., & Schmid, S. M. (2002b). The eastern Tonale fault zone: A 'natural laboratory' for crystal plastic deformation of quartz over a temperature range from 250 to 700°C. *Journal of Structural Geology*, *24*, 1861–1884. https://doi.org/10.1016/S0191-8141(02)00035-4

Topuz, G., Candan, O., Zack, T., & Yılmaz, A. (2017). East Anatolian plateau constructed over a continental basement: No evidence for the East Anatolian accretionary complex. *Geology*, *45*, 791–794. https://doi.org/10.1130/G39111.1

Topuz, G., Göçmengil, G., Rolland, Y., Çelik, Ö. F., Zack, T., & Schmitt, A. K. (2013). Jurassic accretionary complex and ophiolite from northeast Turkey: No evidence for the Cimmerian continental ribbon. *Geology*, *41*, 255–258. https://doi.org/10.1130/G33577.1

Trexler, C.C., 2018, Structural investigations of the tectonic history of the western Greater Caucasus Mountains, Republic of Georgia [PhD thesis]: University of California, Davis, 260 p.

Tullis, J., & Yund, R. A. (1977). Experimental deformation of dry Westerly granite. *Journal of Geophysical Research*, *82*, 5705–5718. https://doi.org/10.1029/JB082i036p05705

Vasey, D., Cowgill, E., Roeske, S., Niemi, N., Godoladze, T., Skhirtladze, I., & Gogoladze, S. (2020), Evolution of the greater Caucasus basement and formation of the Main Caucasus Thrust, Georgia, v4, UC Davis, Dataset, https://doi.org/10.25338/B8D61N

Vavra, G., Gebauer, D., Schmid, R., & Compston, W. (1996). Multiple zircon growth and recrystallization during polyphase Late Carboniferous to Triassic metamorphism in granulites of the Ivrea Zone (Southern Alps): An ion microprobe (SHRIMP) study. *Contributions to Mineralogy and Petrology*, *122*, 337–358. https://doi.org/10.1007/s004100050132

Vermeesch, P. (2012). On the visualisation of detrital age distributions. *Chemical Geology*, *312–313*, 190–194. https://doi.org/10.1016/j.chemgeo.2012.04.021

Vermeesch, P. (2018). IsoplotR: A free and open toolbox for geochronology. *Geoscience Frontiers*, *9*, 1479–1493. https://doi.org/10.1016/j.gsf.2018.04.001

Vermeesch, P., Resentini, A., & Garzanti, E. (2016). An R package for statistical provenance analysis. *Sedimentary Geology*, *336*, 14–25. https://doi.org/10.1016/j.sedgeo.2016.01.009

Villa, I. M., Bucher, S., Bousquet, R., Kleinhanns, I. C., & Schmid, S. M. (2014). Dating polygenetic metamorphic assemblages along a transect across the Western Alps. *Journal of Petrology*, *55*, 803–830. https://doi.org/10.1093/petrology/egu007

Villa, I. M., Hermann, J., Müntener, O., & Trommsdorff, V. (2000). $^{39}Ar–^{40}Ar$ dating of multiply zoned amphibole generations (Malenco, Italian Alps). *Contributions to Mineralogy and Petrology*, *140*, 363–381. https://doi.org/10.1007/s004100000197

Vincent, S. J., Braham, W., Lavrishchev, V. A., Maynard, J. R., & Harland, M. (2016). The formation and inversion of the western Greater Caucasus Basin and the uplift of the western Greater Caucasus: Implications for the wider Black Sea region. *Tectonics*, *35*, 2948–2962. https://doi.org/10.1002/2016TC004204

Vincent, S. J., Carter, A., Lavrishchev, V. A., Rice, S. P., Barabadze, T. G., & Hovius, N. (2011). The exhumation of the western Greater Caucasus: A thermochronometric study. *Geological Magazine*, *148*, 1–21. https://doi.org/10.1017/S0016756810000257

Vincent, S. J., Saintot, A., Mosar, J., Okay, A. I., & Nikishin, A. M. (2018). Comment on "Relict basin closure and crustal shortening budgets during continental collision: An example from Caucasus sediment provenance" by Cowgill et al. (2016). *Tectonics*, *37*, 1006–1016. https://doi.org/10.1002/2017TC004515

Vincent, S. J., Somin, M. L., Carter, A., Vezzoli, G., Fox, M., & Vautravers, B. (2020). Testing models of Cenozoic exhumation in the Western Greater Caucasus. *Tectonics*. https://doi.org/10.1029/2018TC005451

Wang, C. Y., Campbell, I. H., Stepanov, A. S., Allen, C. M., & Burtsev, I. N. (2011). Growth rate of the preserved continental crust: II. Constraints from Hf and O isotopes in detrital zircons from Greater Russian Rivers. *Geochimica et Cosmochimica Acta*, *75*, 1308–1345. https://doi.org/10.1016/j.gca.2010.12.010

White, S. (1977). Geological significance of recovery and recrystallization processes in quartz. *Tectonophysics*, *39*, 143–170. https://doi.org/10.1016/0040-1951(77)90093-2

Yilmaz, A., Adamia, S., Chabukiani, A., Chkhotua, T., ErdoĞan, K., Tuzcu, S., & KarabiyikoĞlu, M. (2000). Structural correlation of the southern Transcaucasus (Georgia)-Eastern Pontides (Turkey). *Geological Society, London, Special Publications*, *173*, 171–182. https://doi.org/10.1144/GSL.SP.2000.173.01.08

Zanchetta, S., Berra, F., Zanchi, A., Bergomi, M., Caridroit, M., Nicora, A., & Heidarzadeh, G. (2013). The record of the Late Palaeozoic active margin of the Palaeotethys in NE Iran. *Constraints on the Cimmerian orogeny: Gondwana Research*, *24*, 1237–1266. https://doi.org/10.1016/j.gr.2013.02.013

Zaridze, G. M. (1959). Association of ore bodies in granitoids of the Caucasus and the genesis of these rocks. *International Geology Review*, *1*, 29–40. https://doi.org/10.1080/00206815909473525

Zonenshain, L. P., & Le Pichon, X. (1986). Deep basins of the Black Sea and Caspian Sea as remnants of Mesozoic back-arc basins. *Tectonophysics*, *123*, 181–211. https://doi.org/10.1016/0040-1951(86)90197-6